Endothelial-to-mesenchymal transition in the fetoplacental macrovasculature and microvasculature in pregnancies complicated by gestational diabetes

Running title: EndMT in the fetoplacental macro- and micro-vasculature in GDM

Authors: Abigail R. Byford[1$*], Georgia Fakonti[1$], Ziyu Shao[1], Sharanam Soni[1], Sophie L. Earle[1], Muath Bajarwan[1], Lara C. Morley[1], Beth Holder[2], Eleanor M. Scott[3], Karen Forbes[1*].

*Corresponding authors

[$]These authors contributed equally.

[1]Discovery and Translational Science Department, Leeds Institute of Cardiovascular and Metabolic Medicine, Faculty of Medicine and Health, University of Leeds, Leeds, LS2 9JT

a.r.byford@leeds.ac.uk; umgf@leeds.ac.uk; mr23zs@leeds.ac.uk; sharanam.soni@postgrad.manchester.ac.uk; s.l.earle@leeds.ac.uk; ummab@leeds.ac.uk; l.c.morley@leeds.ac.uk; k.a.forbes@leeds.ac.uk

[2]Institute of Reproductive and Developmental Biology (IRDB), Imperial College London, London, UK b.holder@imperial.ac.uk

[3]Clinical and Population Sciences, Leeds Institute of Cardiovascular and Metabolic Medicine, Faculty of Medicine and Health, University of Leeds, Leeds, LS2 9JT; e.m.scott@leeds.ac.uk

Key Points

- Gestational diabetes mellitus (GDM) has been linked to altered placental vascularisation, fibrosis, and endothelial dysfunction.
- Endothelial-to-mesenchymal transition (EndMT) is a process where endothelial cells adopt a mesenchymal phenotype. Disruptions in EndMT have been linked to vascular complications in diabetes, but EndMT in GDM has not been investigated.
- TGF-β2 and IL-1β induced morphological and molecular changes consistent with EndMT in GDM and non-GDM HUVECs. Whilst the expression of EndMT mediators, *VWF*, *TGFBR1, IL1B* and *IL1R1* were diminished in GDM HUVECs, all other hallmarks of EndMT were similar.
- Transcriptional regulators of EndMT, Slug and Snail, were detected in the human term placental stroma. Despite a reduction in endothelial markers, *PECAM1, VWF* and *CDH5*, and *SNAI2*, *TGFB2/3* and *TGFBR2* in GDM placenta, there was no change in mesenchymal markers or other EndMT regulators.
- This suggests that whilst there may be some changes to EndMT in GDM, the endothelial and vascular dysfunction are unlikely to be explained fully by alterations in EndMT.

Abstract

Gestational diabetes mellitus (GDM) is linked to altered fetal development and an increased risk of offspring developing cardiometabolic diseases in adulthood. The mechanisms responsible are unclear however, GDM is associated with altered fetoplacental vascularisation, fibrosis, and endothelial dysfunction. In non-pregnant individuals with diabetes, similar vascular changes are attributed to disruptions in endothelial-to-mesenchymal transition (EndMT) ~~is~~ a key process where endothelial cells adopt a mesenchymal phenotype. Here, we assess whether alterations in the fetoplacental macro- and micro-are attributed to EndMT, using human umbilical vein endothelial cells (HUVECs) and human term placental tissue, respectively. TGF-β2 and IL-1β induced morphological and molecular changes consistent with EndMT in both GDM and non-GDM HUVECs. The ability of TGF-β2 and IL-1β to alter

expression of known EndMT regulators, *VWF*, *TGFBR1, IL1B* and *IL1R1* was diminished in GDM HUVECs, however, all other hallmarks of EndMT were similar. In placental villous tissue, Slug and Snail, two key transcriptional regulators of EndMT, were detected in the villous stroma, suggesting that EndMT likely occurs in the placental microvasculature. We observed a reduction in endothelial marker genes *PECAM1*, *VWF,* and *CDH5* in GDM placentas, suggesting reduced placental vascularisation. This was accompanied by a reduction in EndMT regulators *SNAI2, TGB2, TGFB3,* and *TGFBR2,* however, there was no change in mesenchymal markers or other EndMT regulators. This suggests that there may be some alterations in EndMT in GDM but this is unlikely to fully explain the endothelial dysfunction and altered vascularisation that occurs in the fetoplacental vasculature in pregnancies complicated by GDM.

Keywords: Gestational diabetes mellitus, GDM, endothelial-to-mesenchymal transition, placenta, umbilical cord, fetoplacental endothelium, macrovasculature, microvasculature

Introduction

Gestational diabetes mellitus (GDM) is defined by hyperglycaemia with onset during pregnancy and its prevalence is increasing with an estimated 14% of pregnancies affected globally (Wang *et al.*, 2022). Although this hyperglycaemia can be controlled during pregnancy and usually resolves postpartum, GDM has been linked to impaired fetal cardiac development and function, increased rates of congenital heart disease, and an increased risk of developing cardiometabolic diseases in adulthood (Balsells *et al.*, 2012; Venkataraman *et al.*, 2016; Kramer *et al.*, 2019; Aguilera *et al.*, 2021; Depla *et al.*, 2021; Al-Biltagi *et al.*, 2021; Liu *et al.*, 2024; Chen *et al.*, 2024). Despite this, the underlying mechanisms of how GDM causes these effects in offspring is largely unknown. However, defects in fetal cardiac development and rates of long-term cardiovascular complications in offspring are linked to alterations in the fetoplacental vasculature, including endothelial dysfunction (Diniz *et al.*, 2023).

In the human placenta, the microvasculature is comprised of the fetal capillaries residing in the chorionic villi, which function along with the trophoblast, to transfer nutrients, oxygen, and waste between the maternal and fetal circulation (Wang & Zhao, 2010; Junaid *et al.*, 2014). The macrovasculature is comprised of the chorionic plate vessels and umbilical cord, which transport the nutrients, oxygen, and waste between the placenta and fetus (Wang & Zhao, 2010; Junaid *et al.*, 2014). Alterations in both the macro- and micro- fetoplacental vasculature have been reported in pregnancies complicated by GDM (Sobrevia *et al.*, 2011; Byford *et al.*, 2021). These reported alterations include: villous immaturity (Daskalakis *et al.*, 2008), altered vascularisation (Stoz *et al.*, 1988; Calderon *et al.*, 2007; Daskalakis *et al.*, 2008; Jirkovská *et al.*, 2012; Akarsu *et al.*, 2017; Troncoso *et al.*, 2017), fibrosis (Bhattacharjee *et al.*, 2017; Ehlers *et al.*, 2021), endothelial dysfunction (Zhou *et al.*, 2016; Wang *et al.*, 2023*b*) and impaired endothelial barrier function (Cvitic *et al.*, 2018; Villota *et al.*, 2021), which have also been linked to altered fetal heart development (Anbara *et al.*, 2019; Gordon *et al.*, 2022; Diniz *et al.*, 2023). Therefore, understanding the mechanisms for placental vascular dysfunction in GDM is of clear importance.

Placental vascular development is dependent on vasculogenesis, where mesenchymal cells differentiate into endothelial cell and haematopoietic cell progenitors, forming angiogenic cell cords and eventually the primitive capillary network (Demir *et al.*, 2007). Further expansion of the placental vascular network is dependent on angiogenesis, which requires both endothelial cell proliferation and migration (James *et al.*, 2022). In other systems, this process is dynamic, and endothelial-to-mesenchymal transition (EndMT), the transdifferentiation process of endothelial cells towards a mesenchymal phenotype (Piera-Velazquez & Jimenez, 2019), can occur. Cells undergoing EndMT have a more proliferative and migratory phenotype (Piera-Velazquez & Jimenez, 2019; Bischoff, 2019), thus is it possible that EndMT could play a significant role in endothelial cell proliferation and migration in placental vascular development. Other hallmarks of EndMT include a change in morphology to elongated, spindle shaped cells, loss of cell junction molecules, such as VE-cadherin, loss of endothelial markers, and an increase in mesenchymal and myofibroblast markers, such as transgelin and alpha smooth muscle actin (αSMA) (Pinto *et al.*, 2016; Piera-Velazquez & Jimenez, 2019). ~~Modulated by two key transcription factors, Slug and Snail,~~ EndMT has been shown to be induced by members of the transforming growth factor-β (TGF-β) family, pro-inflammatory cytokines, such as interleukin-1 beta (IL-1β), and microRNAs (miRNAs) (Pérez *et al.*, 2017; Singh *et al.*, 2024). In the canonical EndMT signalling pathway, TGF-β binds to heterodimeric TGF-β type I (TGF-βR1) and type II (TGF-βR2) receptor complex on the cell surface to induce phosphorylation of Smad proteins, which are then translocated to the nucleus, to activate the transcription factors Snail and Slug, which in turn regulate the transcription of EndMT target genes (Singh *et al.*, 2024).

EndMT was first described in the developing heart where it plays an essential role in valve formation and heart septation (Markwald *et al.*, 1975, 1977), and disruptions in EndMT give rise to congenital heart defects (Anbara et al., 2019). More recently, Boss and colleagues have described EndMT in first-trimester placental endothelial cells, suggesting that EndMT may also play a key role in placental development (Boss *et al.*, 2023), but this remains to be further explored. Given that EndMT is important during fetal heart development, is altered in congenital heart defects, and similar

developmental processes occur in the developing fetal heart and placenta (Mahadevan *et al.*, 2023), EndMT in the fetoplacental vasculature warrants further investigation.

Increasing evidence also indicates that EndMT is involved in disease processes, particularly in diabetes, where disrupted EndMT contributes to cardiovascular diseases and other vascular pathologies associated with endothelial dysfunction and fibrosis (Kovacic *et al.*, 2019; Wang *et al.*, 2023*a*). It is therefore possible that exposure to a diabetic environment *in utero* also impacts EndMT, vascularisation and associated processes in the developing placenta and fetus, however, to our knowledge, this has not been investigated. Here, we assess whether vascular dysfunction in the diabetic placenta could potentially be attributed to changes in EndMT. Using human umbilical cord endothelial cells (HUVECs) and placental villous tissue from GDM and non-GDM pregnancies we assess whether a diabetic environment *in utero* has the potential to influence EndMT in the fetoplacental macro- and micro- vasculature, respectively. We then assess whether a GDM environment alters EndMT by exposing both GDM and non-GDM HUVECs to known inducers of EndMT.

Methods

Placenta and umbilical cord collection and processing

Healthy pregnant women or women diagnosed with GDM, with singleton term deliveries (between 38-41 weeks' gestation) were recruited at the Leeds Teaching Hospital NHS trust (London - Riverside Research Ethics Committee; REC reference: 18/LO/0067; IRAS project ID: 234385) or at St. Mary's Hospital, Manchester University NHS Foundation Trust (Northwest Research Ethics Committee; REC reference: 08/H1010/55). All participants gave written informed consent and human tissue processing, data curation and analysis, was conducted in accordance with Declaration of Helsinki guidelines and the Human Tissue Act. GDM diagnosis was confirmed through an oral glucose tolerance test in women with risk factors as detailed within the National Institute of Clinical Excellence Diabetes in Pregnancy guideline (NICE, 2015). Either a fasting plasma glucose level of 5.6 mM or above or a 2-hour post-prandial glucose level of 7.8 mM or above is diagnostic of GDM. In women with previous GDM, this would be conducted as soon as possible after booking and repeated at 24-28 weeks gestation if the first was negative. In women with other risk factors for GDM, a single screening test was conducted at 24-28 weeks gestation. Human term placentas and umbilical cords were collected within 30 minutes following delivery. Umbilical cords for HUVECs and placental tissue were processed from different patients. All umbilical cords were collected from caesarean sections, and placentas were collected from both vaginal and caesarean deliveries (**Table 3 and 4**).

For processing of placental tissue, the fetal membranes and umbilical cord were removed, a sample of 5 cm^2 full thickness was collected from the centre (close to umbilical cord insertion), middle (between umbilical cord and edge), and edge of the placenta, to represent the entire organ. The samples were then washed with sterile phosphate buffered saline (PBS; Sigma-Aldrich, Cat #D8537) to remove maternal blood. The basal and chorionic plates were then removed from each sample. For histology, a full thickness tissue section from the centre, middle, and edge were stored in 10% neutral buffered formalin (NBF) (Sigma-Aldrich, Cat #HT501128) at 4°C. After 48 hours NBF was removed,

replaced with 70% ethanol, and stored at 4°C until the tissue was processed. For RNA, tissue pieces from the same centre, middle, and edge samples were further dissected and small pieces from each area were pooled and placed in RNALater (Merck, Cat #R0901- 500ML) for 48 hours, before being snap frozen in liquid nitrogen and stored at -80°C. Maternal demographic and pregnancy outcome information were recorded and birthweight centiles were calculated using the World Health Organisation fetal growth calculator https://srhr.org/fetalgrowthcalculator/, which considered gestational age, birthweight, and fetal sex. Large-for-gestational age (LGA) infants were defined as a birthweight centile $\geq$ 90.

Human Umbilical Vein Endothelial Cell (HUVEC) isolation

HUVECs were isolated from umbilical cords derived from non-GDM (n=6) and GDM (n=5) pregnancies. The umbilical cord was removed from the placenta and placed in sterile PBS (Gibco, Cat #D8537). The umbilical vein was then cannulated and flushed with 20 mL of PBS to remove blood. Following this, 5 mL of 0.1% collagenase type II (Gibco, Cat #17101-015) prepared in Hank's Buffer (Sigma-Aldrich, Cat #H9259) was flushed through the vein, and the end of the cord was clamped using a cord clamp, before filling with an additional 5 mL of collagenase. The cord was clamped at the other end and incubated for 20 minutes at 37^{o}C. The lower cord clamp was removed and placed over a 50 mL falcon tube and flushed with 5 mL of Endothelial Cell Growth Medium 2 (EGM-2) (Promocell, Cat #C22110), with 1% Antibiotic and Antimitotic (Gibco, Cat #15240-062). The suspension was centrifuged for 6 minutes at 256 xG and the supernatant removed. The pellet was then resuspended in 2 mL of EGM-2 and centrifuged again for 6 minutes at 256 xG. This step was repeated twice, and the final pellet was resuspended in 5 mL of EGM-2 and plated into a T25 flask. Half of the medium was refreshed after 24 hours and all the medium was refreshed after a further 48 hours.

HUVEC cell culture

Primary HUVECs or commercial HUVECs (Promocell, Cat #C-12203, Lot #494Z025) (passage 2-6) were cultured in a humidified incubator at 37°C in 5% CO_2, 20% O_2 in EGM-2 with 1% Antibiotic and

Antimitotic (Gibco, Cat #15240-062). HUVECs were passaged at 80-90% confluency using Accutase solution (Sigma-Aldrich, Cat #A6964 or Promocell, Cat # C-41310), and centrifuged at 220 xG for 3 minutes. The supernatant was removed, and the cell pellet was resuspended in fresh EGM-2 before seeding. Medium was refreshed every 2-3 days.

Placental mesenchymal stromal cell (pMSC) culture

Placental mesenchymal stromal cells (pMSCs) were used as a mesenchymal cell positive control (n=7; passage 2-6). Uncomplicated human term placentas were collected from the Leeds Teaching Hospital NHS trust (London - Riverside Research Ethics Committee; REC reference: 18/LO/0067; IRAS project ID: 234385) as described above. pMSCs were isolated and characterised as previously described (Pelekanos *et al.*, 2016; Kennedy, 2022). Briefly, pMSCs were isolated using enzymatic digestion and were characterised using a human mesenchymal stem cell flow cytometry kit (R&D Systems, Cat #FMC002) and tri-lineage differentiation (Kennedy, 2022). pMSCs were cultured in a humidified incubator at 37°C in 5% CO_2, 20% O_2 in low glucose DMEM (Gibco, Cat #11885-092) supplemented with 10% FBS (Gibco, Cat #10270-106), 1% Antibiotic and Antimitotic (Gibco, Cat #15240-062), and 1% Non-Essential Amino Acids (NEAA; Gibco, Cat #11140035). pMSCs were passaged using TrypLE Express (Gibco, Cat #12563-029), which was inactivated with medium before seeding. Medium was refreshed every 2-3 days.

Confirmation of HUVEC purity using flow cytometry

HUVECs (passage 3-6) were characterised using flow cytometry. All centrifugation steps were performed at 220 xG for 3 minutes. Once cells had reached 90-100% confluency they were removed from tissue culture flasks using Accutase solution (Sigma-Aldrich, Cat #A6964) and were centrifuged. The supernatant was removed, and the cell pellet was resuspended in 1 mL staining buffer (R&D Systems, Cat #FC001), which contains BSA to minimise non-specific staining and the metabolic inhibitor sodium azide as a preservative. A total of 100,000 cells were added to each tube. For blocking, 20 µL of Fc receptor blocking reagent, which blocks non-specific binding of antibodies to

human Fc receptor-expressing cells (Miltenyi Biotec, Cat #130-059-901, RRID:AB_2892112), was added to each tube and incubated for 10 minutes at 4°C. The cells were then centrifuged and incubated with the following fluorescently labelled antibodies: CD31-FITC (1:50, Miltenyi Biotec, Cat #130-110-668, Lot #5240600353, RRID:AB_2657279) and CD144-PE (1:50, Miltenyi Biotec, Cat #130-118-495, Lot #5240800873, RRID:AB_2751528) either alone (fluorescence minus one controls; FMOs) or in combination for 15 minutes at 4°C. An additional tube of cells in staining buffer without antibodies was used as an unstained control. Cells were then washed and resuspended in 200 µL of staining buffer for flow analysis using the Cytoflex S Flow Cytometer (Beckman). A gating strategy was applied to remove debris and doublets, and 10,000 events were recorded per tube.

Flow cytometry analysis was performed using CytExpert (Version 2.4.0.28). Following debris and doublet exclusion, the percentage of cells expressing both CD31 and CD144 was measured, using the FMO control to aid gating (**Figure 1Ai**).

EndMT induction in HUVECs

Other studies have used different methodologies to induce EndMT in endothelial cells, *in vitro,* including TGF-β1, TGF-β2, IL-1β, either alone or in combination (Maleszewska *et al.*, 2013; Pinto *et al.*, 2016; Ferreira *et al.*, 2019; Terzuoli *et al.*, 2020; Chen *et al.*, 2023; Zhu *et al.*, 2023; Bronson *et al.*, 2023). Therefore, to determine the best *in vitro* method to induce EndMT, commercial HUVECs were cultured in control medium (EGM-2 only) or EGM-2 containing either TGF-β1 (10 ng/mL; Merck, Cat #H8541-5UG), TGF-β2 (10 ng/mL; Biolegend, Cat #583301, Lot #B397313 and #B415636), TGF-β1 (10 ng/mL) with IL-1β (10 ng/mL; Biolegend, Cat #579404, Lot #B398847), or TGF-β2 (10 ng/mL) with IL-1β (10 ng/mL) for 6 days (n=3). Following initial optimisation of conditions for EndMT, further experiments were conducted using TGF-β2 (10 ng/mL) in combination with IL-1β (10 ng/mL) for 6 days (n=6). For all EndMT experiments, medium was replenished every 2-3 days. Cells were seeded at 1,000 cells/cm^2 in either 6-well plates, or in 24-well plates containing glass coverslips. On day 6, cells were washed with PBS and harvested for RNA isolation or fixed with 4% paraformaldehyde for 20 minutes

followed by PBS washing for immunocytochemistry. Cells were imaged using a Euromex Oxion Inverso microscope with a 10X objective.

RNA Isolation

For RNA isolation from HUVECs and pMSCs, cells were first washed with PBS. Total RNA was extracted using the miRNeasy Advanced Mini kit for tissues and cells (Qiagen, Cat #217604), according to manufacturer's instructions. One-well of a 6-well plate was used per condition/sample. This included a gDNA eliminator spin column, to remove potential contaminating gDNA. All centrifugation steps were performed at 12,000 xG, except for the final steps to dry the membrane and elute RNA, which were performed at maximum speed. RNA was eluted in 40 µL of nuclease-free water and stored at -80°C.

For RNA isolation from human term placental tissue, total RNA was isolated using the mirVana™ miRNA isolation kit (Thermo Fisher Scientific, Cat #AM1561) following manufacturer's instructions. Briefly, 0.25 g of snap frozen tissue was lysed and homogenised using 300 µL of lysis/binding buffer and 30 µL of miRNA homogenate additive. Phase separation was performed using 300 µL of acid-phenol:chloroform (Ambion, Cat #AM9720). All centrifugation steps were performed at 10,000 xG except for elution which was performed at maximum speed in 100 µL of pre-heated (95°C) nuclease-free water. The recovered RNA was then purified using the RNA clean and concentrator-5 kit (Zymo Research, Cat #R1014), following manufacturer's instructions. To remove potential contaminating gDNA, 40 µL of isolated RNA was incubated with 5 µL Dnase I and 5 µL DNA Digestion Buffer for 15 minutes at room temperature. All centrifugation steps were performed at 10,000 xG. RNA was eluted in 15 µL of nuclease-free water and stored at -80°C.

For all RNA samples, concentration and quality (260:280 and 260:230 ratios) were assessed using the Nanodrop (DeNovix, DS-11).

RT-qPCR

RT-qPCR was used to measure gene expression. For complementary DNA (cDNA) synthesis, the Affinity Script Multiple Temperature cDNA Synthesis Kit (Agilent, Cat #200436) was used, according to the manufacturer's instructions. Samples were prepared by adding 100 ng RNA to nuclease-free water in a total volume of 12.5 µL. No template and no reverse transcriptase controls were also prepared with nuclease-free water to replace the RNA or the reverse transcriptase enzyme, respectively. Samples were placed in a thermal cycler (Applied Biosystems Venti 96 Well, ThermoFisher) and were heated to 25°C for 10 minutes, 42°C for 60 minutes and 70°C for 15 minutes, with a final indefinite hold at 4°C. Samples were stored at -20°C.

RT-qPCR was conducted using specific primers at a final concentration of 0.36 µM (**Table 1**) and the Brilliant III Ultra-Fast SYBR Green Master Mix kit (Agilent, Cat #600882), according to manufacturer's instructions. cDNA was diluted 1:10. Samples were loaded in duplicate into white-bottom qPCR plates. Plates were loaded into a LightCycler 96 Instrument (Roche). Plates were preincubated at 95°C for 3 minutes, followed by 40 cycles of 2 step amplification: 95°C for 20 seconds, then a primer specific annealing step (**Table 1**) for 20 seconds. This was followed by a final cycle of 95°C for 1 minute, 55°C for 30 seconds and 95°C for 1 second to generate dissociation curves to confirm the PCR product. The data was then analysed using the LightCycler 96 1.1 software (Roche). Data were acquired as an amplification curve and raw cycle threshold (Ct) values which were used to calculate the relative gene expression via the $2^{(-Ct)}$x100 method, normalising against the housekeeping gene *YWHAZ*.

264 **Table 1 – Primers used for RT-qPCR.**

Gene Name	Primer	Sequence (5'->3')	Annealing Temperature (°C)	Product Length	Reference
ACTA2 (αSMA)	**Forward primer**	TGAGCGTGGCTATTCCTTCGT	65	108	Designed
	Reverse primer	GCAGTGGCCATCTCATTTTCAA			
ACVRL1 (ALK1)	**Forward primer**	TGCAGTGTTGCATCGCCGAC	62	269	Designed
	Reverse primer	TGGGGTCATTGGGCACCACA			
CDH5 (VE-Cadherin)	**Forward primer**	CAGGCAGTCCAACGGAACAGAAA	60	863	Designed
	Reverse primer	CGACAAATGTGTACTTGGTCTGGGT			
IL1B	**Forward primer**	CACCAATGCCCAACTGCCTGC	60	219	Designed
	Reverse primer	TGCTCATCAGAATGTGGGAGCGA			
IL1R1	**Forward primer**	AGAGGAAAACAAACCCACAAGG	55	106	(Bellehumeur *et al.*, 2009)
	Reverse primer	CTGGCCGGTGACATTACAGAT			
NT5E (CD73)	**Forward primer**	CTAGCGCAACCACAAACCATAC	65	79	Designed
	Reverse primer	CTGGGTCCTCTCTGAGTCTCG			
PECAM1 (CD31)	**Forward primer**	GCTGAGTCTCACAAAGATCTAGGA	57	91	(Böhrnsen & Schliephake, 2016)
	Reverse primer	ATCTGCTTTCCACGGCATCA			
SMAD2	**Forward primer**	GGAGCAGAATACCGAAGGCA	60	128	(Yu *et al.*, 2009)
	Reverse primer	CTTGAGCAACGCACTGAAGG			
SMAD3	**Forward primer**	AGAAGACGGGGCAGCTGGAC	60	511	(Yu *et al.*, 2009)
	Reverse primer	GACATCGGATTCGGGGATAG			
SMAD4	**Forward primer**	GCATCGACAGAGACATACAG	60	411	(Yu *et al.*, 2009)
	Reverse primer	CAACAGTAACAATAGGGCAG			
SNAI1 (Snail)	**Forward primer**	CTTCCAGCAGCCCTACGAC	60	71	(Terzuoli *et al.*, 2020)
	Reverse primer	CGGTGGGGTTGAGGATCT			
SNAI2 (Slug)	**Forward primer**	ACTCCGAAGCCAAATGACAA	60	119	(Xu *et al.*, 2015)
	Reverse primer	CTCTCTCTGTGGGTGTGTGT			
TAGLN (Transgelin)	**Forward primer**	GGCTGAAGAATGGCGTGATT	60	108	Designed
	Reverse primer	TCTGCTTGAAGACCATGGAGG			
TGFB1	**Forward primer**	GGTTGAGCCGTGGAGGGGAAAT	60	280	Designed
	Reverse primer	ATGTACAGCTGCCGCACGCA			
TGFB2	**Forward primer**	GTTCGATTTGACGTCTCAGCAAT	60	112	(Yoshimatsu *et al.*, 2020)
	Reverse primer	CAATCCGTTGTTCAGGCACTCT			
TGFB3	**Forward primer**	ATGACCCACGTCCCCTATCA	60	113	(Yoshimatsu *et al.*, 2020)
	Reverse primer	TCCGACTCGGTGTTTTCCTG			
TGFBR1 (ALK5)	**Forward primer**	AACTTGCTCTGTCCACGGCG	60	238	Designed
	Reverse primer	ACTTCAGGGGCCATGTACCTTT			
TGFBR2	**Forward primer**	TGGCTCAACCACCAGGGCAT	60	96	Designed
	Reverse primer	TGCCACACACTGGGCTGTGA			
VWF	**Forward primer**	CCCATTTGCTGAGCCTTGT	57	141	(Wang *et al.*, 2018)
	Reverse primer	GGATGACCACCGCCTTTG			
YWHAZ	**Forward primer**	ACTTTTGGTACATTGTGGCTTCAA	55	94	Designed
	Reverse primer	CCGCCAGGACAAACCAGTAT			

265

266

Immunocytochemistry and fluorescence microscopy

For intracellular staining, cells cultured on coverslips were permeabilized with PBS containing 0.1% Triton-X100 (Sigma-Aldrich, Cat #X100-500ML) for 30 minutes. Coverslips were then washed 3 times with PBS and blocked with 5% BSA (BSA; Roche, Cat #10735078001) in PBS for 30 minutes at room temperature. Following blocking, cells were incubated with primary antibodies diluted in 5% BSA, specific for endothelial and mesenchymal markers, EndMT regulators and proliferative markers (**Table 2**) overnight at 4°C. After incubation, coverslips were washed 3 times with PBS to remove unbound primary antibody and were incubated with appropriate fluorescently labelled secondary antibodies, diluted in 5% BSA, (**Table 2**) for 1.5 hours at room temperature. Coverslips were then washed 3 times with PBS to remove unbound secondary antibody and were then mounted onto fresh microscope slides using Fluoromount-G with 4',6-diamidino-2-phenylindole (DAPI) (Southern Biotech, Cat #0100-20). Negative controls included coverslips incubated with an isotype-specific control or with secondary antibody only.

Visualisation and imaging of coverslips was performed using the Olympus IX83 microscope with a 20x/0.75 U PlanS Apo objective. For each coverslip, three regions of interest (ROI) were imaged. The same exposure times were used for each antibody across all samples. Images were analysed using QuPath (v. 0.5.1), a software for digital bioimage analysis (Bankhead *et al.*, 2017). Firstly, the brightness and contrast settings for each channel were adjusted and applied across all images. A pixel classifier threshold was set to detect the cells in each ROI. The fluorescence intensity was then determined using the intensity features tool. The intensity was calculated per pixel, to account for differing numbers and sizes of cells in each ROI/image. To measure proliferation, the positive cell detection tool was used to identify all DAPI-positive and Ki67-positive cells and the percentage of Ki67 positive cells was then calculated.

Table 2 – Antibodies used for immunocytochemistry and/or immunohistochemistry.

Protein	Labels	Host	Stock Concentration	Dilution	Final Concentration	Manufacturer	Cat #	Lot #; RRID
CD31	Endothelial	Mouse	201 µg/mL	1:100	2.01 µg/mL	Dako	M0823	41526059; AB_2114471
VWF	Endothelial	Mouse	140 µg/mL	1:200	0.7 µg/mL	Dako	M0616	20084172 RRID:AB_2216702
VE-Cadherin	Endothelial	Rabbit	105 µg/ml	1:600	0.175 µg/ml	Cell Signalling Technologies	2500	5; RRID:AB_10839118
Transgelin	Mesenchymal	Rabbit	900 µg/mL	1:300	3 µg/mL	Abcam	ab14106	GR3438803-1 AB_443021
αSMA	Mesenchymal	Mouse	1000 µg/mL	1:80	12.5 µg/mL	R&D Systems	MAB1420	IBR0922071 RRID:AB_262054
Ki67	Proliferation	Mouse	46 µg/mL	1:50	0.92 µg/mL	Dako	M7240	20075742; RRID:AB_2142367
Snail	Transcription Factor	Mouse	200 µg/mL	1:100	2 µg/mL	Santa Cruz	SC-271977	K0520 RRID:AB_10709902
Slug	Transcription Factor	Mouse	200 µg/mL	1:100	2 µg/mL	Santa Cruz	SC-166476	A1518 RRID:AB_2191897
Mouse IgG	Isotype Control	Mouse	2000 µg/mL	Various	Various	Vector Labs	I-2000-1	ZG0115; AB_2336354
Rabbit IgG	Isotype Control	Rabbit	5000 µg/mL	Various	Various	Vector Labs	I-1000-5	ZH1201; AB_2336355
Anti-Mouse 488	Secondary	Goat	2000 µg/mL	1:2000	1 µg/mL	Thermofisher Scientific	A11001	2090562; RRID:AB_2534069
Anti-Rabbit 488	Secondary	Goat	2000 µg/mL	1:2000	1 µg/mL	Thermofisher Scientific	A11008	2051237; RRID:AB_143165
Anti-Mouse 568	Secondary	Goat	2000 µg/mL	1:1500	1.3 µg/mL	Thermofisher Scientific	A11031	2026148; RRID:AB_144696
Anti-Rabbit 568	Secondary	Goat	2000 µg/mL	1:1500	1.3 µg/mL	Thermofisher Scientific	A11011	54936A; RRID:AB_143157
Anti-Mouse Biotin	Secondary	Goat	1000 µg/mL	1:200	5 µg/mL	AAT Bioquest	16729	2760781 RRID:AB_3665168
Anti-Rabbit Biotin	Secondary	Swine	510 µg/mL	1:200	2.55 µg/mL	Dako	E0353	20016769; RRID:AB_2737292

Immunohistochemistry

Following fixation in 10% NBF, human placental tissue was dehydrated and cleared using a tissue processor (Lecia, TP1020) and embedded in paraffin wax. Formalin-fixed paraffin-embedded tissue was then cut into 5 µm sections using a microtome (Lecia, RM2125RTF) and transferred onto Poly-L-Lysine coated slides (VWR, Cat #631-0107). Tissue sections were dewaxed and rehydrated using HistoClear (National Diagnostics, Cat #NAT1330) and decreasing concentrations of ethanol (100-70%). Heat-activated antigen retrieval was performed by boiling tissue in 0.01 M sodium citrate buffer (pH 6.0). Immunohistochemistry was performed using specific antibodies for endothelial and

mesenchymal markers and EndMT regulators (**Table 2**), which were incubated overnight at 4°C. After incubation, slides were washed 3 times with tris buffered saline (TBS) to remove unbound primary antibody and were incubated with appropriate biotinylated secondary antibodies (**Table 2**), for 1 hour at room temperature and immunoreactivity was visualised using the avidin-peroxidase method followed by 3, 3'-diaminobenzidine (DAB) as previously described (Forbes *et al.*, 2008). Sections were counterstained with haematoxylin (Sigma-Aldrich, Cat #HHS16) then dehydrated and cleared in HistoClear before mounting with coverslips using DPX (Thermofisher Scientific). Sections were imaged using the Axioscan Z1 Slide Scanner (Zeiss).

Statistical Analysis

Statistical analysis was performed using GraphPad Prism (V. 10.2.0). Data was assessed for normality using quantile-quantile plots and Shapiro-Wilk tests. When continuous data were normally distributed, an unpaired t-test or one-way analysis of variance (ANOVA) followed by a Dunnett's post-hoc test was used. When continuous data was not normally distributed, a Mann-Whitney U test or a Kruskal-Wallis test, followed by a Dunn's post-hoc test was used. For grouped data, a two-way ANOVA was performed, with a Fisher's post-hoc test. Grouped data that were not normally distributed were log transformed and assessed using a two-way ANOVA. For categorical data a Fisher's exact test was used. A p value <0.05 was considered statistically significant.

Results

EndMT markers are expressed in HUVECs

To investigate whether GDM could potentially exert changes to EndMT we first isolated HUVECs from non-GDM (n=6) and GDM pregnancies (n=5; **Table 3**) and assessed expression of EndMT markers. The phenotype of the HUVECs was confirmed using flow cytometry (n=3/group) which demonstrated that the isolated cells from both non-GDM and GDM pregnancies co-expressed CD31 and VE-Cadherin/CD144 (98.57±0.40 % and 99.59±0.24 %, respectively) (**Fig. 1A**), confirming their endothelial phenotype. RT-qPCR demonstrated that, as expected, HUVECs expressed the endothelial genes *PECAM1* (CD31), *VWF,* and *CDH5* (VE-Cadherin; **Fig. 1B i-iii**). There was minimal gene expression of mesenchymal markers, *ACTA2* (αSMA), *TAGLN* (transgelin), and *NT5E* (CD73) compared to isolated placental mesenchymal stromal cells (pMSCs; **Fig. 1B iv-vi**). EndMT transcription factors, *SNAI1* (Snail) and *SNAI2* (Slug), were also expressed at low levels in HUVECs (**Fig. 1B vii-viii**). No differences were observed in expression of mesenchymal markers, EndMT transcription factors, or the majority of endothelial markers, between GDM and non-GDM HUVECs, except for *CDH5* which was higher in GDM HUVECs (p=0.0486; **Fig. 1B iii**).

Table 3 - Maternal and fetal demographic information for HUVEC samples used. Data is presented as the [1]mean ± standard deviation and [2]absolute numbers. Statistical analysis was performed using an unpaired t-test (Maternal Age, Booking BMI, Gestational Age, Placental Weight, Birthweight; normally distributed continuous data) or a Fisher's Exact test (Ethnicity, Parity, Birthweight Class, Fetal Sex; categorical data). Abbreviations: LGA – large for gestational age, AGA – appropriately grown for gestational age, BMI – body mass index, N/A – not applicable. [a] Not available (either no medication is prescribed, or no medication was identified in the medical records and available demographics). All HUVECs were isolated from elective caesarean section deliveries.

	Non-GDM (n=6)	GDM (n=5)	P Value
Maternal age (years)[1]	28.8±4.83	32.4±3.51	P=0.204
Booking BMI (kg/m^2) [1]	23.9±4.20	34.7±8.33	P=0.0204
Ethnicity[2]	Chinese = 1; White British = 4, Indian = 1	African = 1; Indian = 1, Asian (Other) = 1; White British = 2	P=0.740
Gestational age (days) [1]	274.0±1.67	270.6±3.78	P=0.0770
Parity[2]	P0 = 3 P1 = 2 P2 = 1	P0 = 1 P1 = 1 P2 = 1 P3 = 2	P=0.584
Placental weight (g) [1]	403.0±53.0	534.0±47.2	P=0.00210
Birthweight (g) [1]	3335±338.6	3615±262.8	P=0.167
Birthweight centile[1]	42.42±25.50	73.56±20.19	P=0.0546
Birthweight class[2]	AGA = 6	LGA = 1; AGA = 4	P=0.455
Fetal sex[2]	Male = 3; Female = 3	Male = 2; Female = 3	P=1.00
GDM medication[2]	N/A	Metformin = 1; Insulin and Metformin = 2; Not available = 2 [a]	N/A

EndMT potential in HUVECs from GDM and non-GDM pregnancies

Next, we assessed if there is altered EndMT potential in HUVECs from pregnancies complicated by GDM. First, initial experiments were performed to determine the best method for inducing EndMT in HUVECs (**Fig. 2)** and it was established that the combination of TGF-β2 and IL-1β was optimal for EndMT induction in commercial HUVECs (**Fig. 2**), consistent with previous studies (Maleszewska *et al.*, 2013). We then assessed if there were differences between TGF-β2 and IL-1β EndMT induction in HUVECs isolated from GDM and non-GDM pregnancies. Treatment of non-GDM HUVECs with TGF-β2 and IL-1β induced morphological changes consistent with EndMT, where cells were more elongated and spindle-shaped (**Fig. 3A**). This was accompanied by reduced expression of endothelial genes *PECAM1* ($p=0.00140$), *VWF* ($p<0.001$), and *CDH5* ($p<0.001$; **Fig 3B i-iii**) and increased expression of mesenchymal genes *TAGLN* ($p<0.0001$) and *NT5E* ($p<0.001$; **Fig. 3B iv-vi**). Analysis of immunocytochemistry images (**Fig. 3C and D**) demonstrated that treatment exerted similar changes to endothelial and mesenchymal markers in HUVECs from non-GDM pregnancies at the protein level. Specifically, there was reduced protein expression of CD31 ($p=0.0206$), VE-Cadherin ($p<0.001$), and VWF ($p<0.001$) (**Fig. 3C i-iii and D**) and increased levels of transgelin ($p<0.0001$) (**Fig. 3C v and D**). Interestingly, there was no change in *ACTA2* levels (**Fig. 3B iv**) following treatment, but there was a reduction in αSMA protein expression ($p=0.0392$; **Fig. 3C iv**). Proliferation of HUVECs was also assessed using Ki67, revealing that EndMT induction in HUVECs reduced the percentage of Ki67 positive cells (12.25±5.001% compared to 72.29±8.38%, $p<0.0001$; **Fig. 3C vi and D**).

In GDM HUVECs, TGF-β2 and IL-1β exposure also induced EndMT (**Fig. 3**). Whilst cell morphology, (**Fig. 3A**), levels of most endothelial and mesenchymal genes (**Fig. 3B ~~& Supplementary Fig. 4~~**) and proteins (**Fig. 3C and D**), and rates of proliferation (Ki67; **Fig. 3C vi and D**) were comparable with treated non-GDM HUVECs, there were some subtle differences between the groups. Expression of *CDH5* was significantly higher in treated GDM HUVECs than in non-GDM HUVECs ($p=0.00790$; **Fig. 3B iii**), however, this is likely attributed to higher basal levels of *CDH5* in GDM HUVECs (**Fig. 1B iii**) since there was no difference in degree of induction by TGF-β2 and IL-1β (fold change compared to control) in

CDH5 gene expression (~~**Supplementary Fig. 4**~~) or in VE-Cadherin protein expression, which is encoded by the *CDH5* gene in GDM HUVECs (**Fig 3C iii and D**). Interestingly, when we analysed the data (**Fig 3B**) by assessing the fold change, *VWF* gene expression following treatment was lower in GDM compared to non-GDM (p=0.0384 ~~**Supplementary Fig. 4**~~), suggesting induction of EndMT may have less of an impact on *VWF* expression in GDM HUVECs.

Regulators of EndMT are altered in HUVECs from pregnancies complicated by GDM

We next assessed the impact of GDM on expression of key EndMT regulatory molecules in HUVECs. No differences in *TGFB1* (**Fig 4A**), *TGFB3* (**Fig 4C**), *ACVRL1* (ALK1) (**Fig 4E**), *SMAD2* (**Fig 4K**), or *SMAD4* (~~all p>0.05;~~ **Fig. 4M**) were observed between GDM and non-GDM HUVECs whether untreated or following EndMT induction. In both GDM and non-GDM HUVECs, EndMT induction resulted in a reduction in TGFβ Receptor 2 (*TGFBR2*; non-GDM: p=0.00700, GDM: p=0.0220; **Fig. 4F**) and *SMAD3* (non-GDM: p=0.0163; GDM: p=0.0152; **Fig. 4L**) following TGF-β2 and IL-1β treatment. This was accompanied by increased expression of *TGFB2* (non-GDM: p<0.0001; GDM: p<0.0001; **Fig. 4B**), TGF-β Receptor 1 (*TGFBR1*)/activin receptor-like kinase 5 (ALK5; non-GDM: p<0.0001, GDM: p<0.0001; **Fig. D**), *SNAI1* (non-GDM: p=0.0107; GDM: p<0.001; **Fig. 4I**), and *SNAI2* (non-GDM: p=0.0191; GDM: p<0.001; **Fig. 4J**). EndMT induction of *TGFBR1* expression was lower in GDM HUVECs compared to non-GDM HUVECs (p<0.001; **Fig. 4D**). TGF-β2 and IL-1β increased levels of *IL1B* (**Fig. 4G**) and *IL1R* (**Fig. 4H**) expression only in non-GDM HUVECs (p=0.0160 and p=0.00630, respectively), with no change in GDM HUVECs. This suggests that a GDM environment may impact the regulatory mechanisms controlling EndMT in HUVECs.

EndMT markers are expressed in ~~the~~ human placental villous tissue

To determine if GDM has the potential to impact EndMT in placental microvascular endothelial cells, we performed immunohistochemistry for EndMT transcription factors, Snail and Slug, along with endothelial (CD31) and mesenchymal markers (transgelin and αSMA; **Fig. 5A**) in term human placental tissue obtained from GDM and non-GDM pregnancies. As expected, CD31 was localised to the endothelium of placental blood vessels (**Fig. 5A**), transgelin and αSMA were detected in both villous stroma and placental blood vessels. Snail was detected in the villous stroma in both GDM and non-GDM placenta (**Fig. 5A**), whilst Slug was present in trophoblast and villous stroma, particularly surrounding placental vessels, in both non-GDM and GDM placenta (**Fig. 5A**).

We next assessed whether a GDM environment had the potential to influence EndMT in the placenta in term human placental lysates from non-GDM and GDM pregnancies (**Table 4**) by assessing expression of EndMT markers and mediators however, the levels of *NT5E*, *SMAD3,* and *IL1B* were at the lower end of detection, so it was not possible to assess if they were altered between groups. In the GDM placenta, there was a downregulation of endothelial markers *PECAM1* (p=0.00600), *VWF* (p<0.001), and *CDH5* (p=0.0373) (**Fig. 5B i-iii**), as well as downregulation of *SNAI2* (p=0.0121; **Fig. 5C ix**), *TGFB2* (p=0.00390; **Fig. 5C ii**), *TGFB3* (p=0.00270; **Fig. 5C iii**), and *TGFBR2* (p=0.0487; **Fig. 5C vi**) indicating that there may be less EndMT occurring in the GDM placentas. However, when we assessed levels of mesenchymal markers, *TAGLN* and *ACTA2* (**Fig. 5B iv-v**), and other EndMT mediators (**Fig. 5C**), there were no differences ~~(p>0.05)~~. All together this suggests that there is reduced vascularisation in the GDM placentas, that is not a result of elevated EndMT.

Table 4 - Maternal and fetal demographic information for placental samples used Data is presented as the [1]mean ± standard deviation, [2]absolute numbers, and [3]median (25% percentile, 75% percentile). Statistical analysis was performed using an unpaired t-test (Maternal Age, Booking BMI, Gestational Age, Placental Weight, Birthweight; normally distributed continuous data) or Mann-Whitney U test (Birthweight Centile; not normally distributed continuous data) or a Fisher's Exact test (Ethnicity, Parity, Mode of Delivery, Birthweight Class, Fetal Sex; categorical data). Abbreviations: LGA – large for gestational age, AGA – appropriately grown for gestational age, BMI – body mass index, SVD - spontaneous vaginal delivery, VD-ind - induced vaginal delivery, ELCS - elective caesarean section, EMCS - emergency caesarean section, N/A – not applicable. [a]n=17, [b]n=16, [c]Not available (either no medication is prescribed, or no medication was identified in the medical records and available demographics).

	Non-GDM (n=17)	GDM (n=18)	P Value
Maternal Age (years) [1]	29.5±5.32	32.4±4.16	P=0.0791
Booking BMI (kg/m²) [1]	29.3±8.89	30.5±6.03[a]	P=0.653
Ethnicity	White = 12; Black = 1, Asian = 4	White = 8; Asian = 7; Other = 3	P=0.118
Gestational age (days) [1]	274.5±6.96	270.1±5.52[b]	P=0.0507
Parity	P0 = 5 P1 = 6 P2 = 4 P3 = 2	P0 = 3 P1 = 7 P2 = 3 P3 = 2 P≥4 = 3	P=0.534
Mode of delivery	SVD = 6; ELCS = 10, Unknown = 1	SVD = 3; VD-ind = 2; ELCS = 8; EMCS = 4; Unknown = 1	P=0.109
Placental weight (g) [1]	608.6±133.0[b]	665.9±257.2	P=0.429
Birthweight (g) [1]	3810±494.1	3732±629.5	P=0.685
Birthweight Centile[3]	89.9 (46.65, 96.15)	82.40 (42.48, 97.50)[b]	P=0.872
Birthweight Class[2]	AGA = 8; LGA = 9	AGA = 10; LGA = 8	P=0.739
Fetal sex[2]	Male = 9; Female = 8	Male = 9; Female = 8, Unknown = 1	P=1.00
GDM medication[2]	N/A	Metformin = 1; Diet = 1, Not Available = 16[c]	N/A

Discussion

GDM increases the risk of pregnancy complications and is associated with alterations in the fetoplacental micro- and macro- vasculature (Sobrevia *et al.*, 2011; Byford *et al.*, 2021). Here we show that EndMT regulatory markers are present in both the micro- and macro-vasculature of the placenta in non-GDM and GDM pregnancies. Whilst the potential for EndMT induction is not altered in the macrovasculature in GDM, subtle alterations in EndMT regulatory genes occur in the microvasculature.

Induction of EndMT has been widely reported in HUVECs (Maleszewska *et al.*, 2013; Ferreira *et al.*, 2019; Terzuoli *et al.*, 2020; Chen *et al.*, 2023; Bronson *et al.*, 2023), and more recently EndMT was described in first trimester placental endothelial cells, suggesting EndMT may contribute to placental vascular development and function (Boss et al., 2023). As far as we are aware, we are the first to show that EndMT mediators (Snail and Slug) are present in the villous stroma in term human placenta. This suggests that EndMT likely plays a role in maintenance of tissue homeostasis in the placenta and given other documented roles for EndMT, it is likely that this could involve the development and function of placental vessels (Piera-Velazquez & Jimenez, 2019). Boss et al., (2023) also demonstrated that first trimester placental endothelial cells undergoing EndMT can further be induced towards a contractile smooth muscle phenotype, expressing αSMA and calponin, thus another potential role for EndMT in the placenta could be in the regulation of vessel contractility and placental blood flow. However, further studies to assess the role of EndMT in the placenta are required.

In this study, we demonstrated that TGF-β2 and IL-1β-induced EndMT in HUVECs as exemplified by changes in cellular morphology, a reduction in endothelial cell markers, and an increase in mesenchymal markers. This was accompanied by increased expression of *TGFB2, TGFBR1* (ALK5), and the EndMT transcription factors, *SNAI1* and *SNAI2*. This is consistent with other *in vitro* EndMT models (Maleszewska et al., 2013; Ma et al., 2021; Monteiro et al., 2021) (Evrard et al., 2016), suggesting that

EndMT in fetoplacental vasculature is likely mediated through the canonical EndMT signalling pathway, however further work to explore the EndMT signalling mechanisms are required.

In GDM HUVECs, the induction of *TGFBR1, IL1B,* and *IL1R* expression were diminished compared to non-GDM placenta, which is consistent with other studies reporting dysregulation of TGF-β and IL-1β signalling in the GDM placenta (Yener *et al.*, 2007; Vitoratos *et al.*, 2008; Grissa *et al.*, 2010; Zgutka *et al.*, 2024). However, there were no differences in the expression of mesenchymal markers, EndMT transcription factors, nor the majority of endothelial markers following EndMT induction.

Whilst this may suggest that the vascular changes that occur in the GDM placenta are not attributed to EndMT, another possible explanation may be that our study was not powered to assess whether there were differences in EndMT in GDM placenta that could be linked to adverse outcomes in GDM, such as birthweight. GDM is well documented to result in complications of fetal growth, whereby babies are born small or large for gestational age (Drever *et al.*, 2023). Boss and colleagues have demonstrated changes in placental EndMT in fetal growth restriction (FGR) and Aplin and colleagues postulate that EndMT may explain the vascular regression in FGR placenta (Aplin *et al.*, 2015; Boss *et al.*, 2023). This is particularly important to note in the context of our current study given that our HUVECs and placental samples included those from pregnancies with LGA as well as appropriately grown for gestational age (AGA) infants. Whilst we did not assess it in this cohort, the level of maternal glucose control in GDM can affect pregnancy outcomes, including fetal growth (Metzger *et al.*, 2008; Law *et al.*, 2019), and rates of congenital heart disease (Helle *et al.*, 2018), furthermore, hyperglycaemia has been shown to induce EndMT (Tsai *et al.*, 2019; Tian *et al.*, 2021; Li *et al.*, 2023; Meng *et al.*, 2023; Hulshoff *et al.*, 2023; Fu *et al.*, 2024), albeit at supraphysiological levels. ~~Similarly, metformin has been shown to impact on epithelial to mesenchymal transition~~ (Di Matteo *et al.*, 2021)~~.~~ It would therefore be interesting to assess EndMT in the context of ~~a role for EndMT in the regulation of~~ fetal growth and maternal glucose control in future studies.

Another potential explanation for our findings is that a GDM environment has less of an impact on EndMT in placental macrovasculature than in placental microvasculature, given that glucose levels have been shown to be lower in umbilical cord vein than in placenta or maternal circulation (Holme *et al.*, 2015). Moreover, umbilical vessels are known to differ in their structure from placental blood vessels (Lang *et al.*, 2008), and *in vitro* HUVECs have altered morphology and responses to endothelial growth factors compared to placental microvascular endothelial cells (Lang *et al.*, 1993), and there may also be differences in venous and arterial endothelial cells from the umbilical cord (Vega-Tapia *et al.*, 2021). Indeed, our observation that the reduction in endothelial cell marker expression (*PECAM1, VWF,* and *CDH5*) in GDM placental villous tissue was accompanied by a reduction in some EndMT regulators, including *SNAI2*, *TGFB2*, *TGFB3* and *TGFBR2* supports this hypothesis.

However, we saw no changes in mesenchymal markers in the GDM placenta nor in other EndMT regulators which may suggest that these genes have other roles in the placenta. For example, *SNAI2* is also known to regulate vascular remodelling, smooth muscle differentiation, proliferation and migration, and endothelial cell functions during angiogenesis (Zhou *et al.*, 2019), suggesting that altered *SNAI2* in the GDM placenta may be linked to other alterations in vascular development. Similarly, TGF-β, IL-1 and CDH5 (VE-Cadherin) are known to play other roles in angiogenesis, vasculogenesis and endothelial barrier function (Babawale *et al.*, 2000; Leach *et al.*, 2002, 2004; Goumans *et al.*, 2009; Fahey & Doyle, 2019), thus the lower levels of molecules in these pathways in GDM may be linked to alterations in these processes. It would be of interest to expose placental villous tissue to the EndMT induction protocol to assess changes in *SNAI2, CDH5* and other markers. However, studies suggest that vessel integrity is reduced during culture in placental explants (Aplin *et al.*, 2015), which potentially limits the use of explants for studying EndMT, so studies using isolated placental microvascular endothelial cells may be required to address this.

Overall, this study is the first to investigate whether a diabetic environment *in utero* has the potential to influence EndMT in the fetoplacental macro- and micro- vasculature. We show that EndMT markers are present in the human placenta at term, indicating a capacity for EndMT in the placenta. Treatment

with TGF-β2 and IL-1β induced morphological and molecular changes consistent with EndMT in both non-GDM and GDM macrovasculature ~~HUVECs~~. Whilst we observed that GDM may impact the regulatory mechanisms controlling EndMT in the macrovasculature ~~HUVECs~~, we observed no alterations in the level of EndMT induction. In the GDM fetoplacental microvasculature, reduced gene expression of endothelial markers is consistent with altered EndMT, however there were limited changes in mesenchymal markers and other EndMT regulators and further studies are required to explore this. Our data suggests that in GDM, although there may be some changes in EndMT regulatory molecules in the fetoplacental vasculature, alterations in EndMT are unlikely to fully explain the fetoplacental vascular dysfunction and associated complications in the fetus and offspring ~~that~~ pregnancies complicated by GDM.

Author Contributions

K.F conceptualized the study, with input from A.R.B and G.F. K.F and E.S secured funding. K.F, A.R.B, E.M.S and B.H supervised all aspects of the study. Z.S and S.S contributed to experiments and data acquisition. A.R.B and G.F performed experiments and analysed and interpreted all data sets. M.B, S.L.E, and L.C.M contributed to the isolation of HUVECs. A.R.B, G.F, and K.F wrote the manuscript with input from all authors. All authors approved the final version of the manuscript, agree to be accountable for all aspects of the work in ensuring that questions related to the accuracy or integrity of any part of the work are appropriately investigated and resolved; and all persons designated as authors qualify for authorship, and all those who qualify for authorship are listed.

Data Availability Statement

All data underlying the results are available as part of the article and no additional source data are required.

Funding

G.F was funded by a University of Leeds Doctoral Scholarship. L.C.M and S.L.E were supported in part by the Tommy's (The Pregnancy and Baby Charity) Preterm Birth Centre. L.C.M. was supported by a NIHR Academic Clinical Lectureship. M.B is funded by King Saud bin Abdulaziz University for Health Sciences. The work conducted in this study was supported by funding from UK Research and Innovation (UKRI) Medical Research Council (REF:MR/R023166/1; awarded to K.F and Ref: MR/Y003659/1; awarded to K.F and E.S). For the purpose of open access, the authors have applied a CC BY public copyright license to any Author Accepted Manuscript version arising from this submission.

Acknowledgements

We would like to thank Margeurite Kennedy for contributing to the pMSC isolations. Flow cytometry and microscopy was performed in The Bioimaging Core Facility, Faculty of Biological Sciences, University of Leeds. We would like to thank the patients, for the donation of their placentas to the study, and the staff in the delivery units at Leeds General Infirmary and St James University Hospital, Leeds Teaching Hospitals NHS Trust and St Mary's Hospital, Manchester University NHS Foundation Trust (MFT).

Competing Interests

No authors have any conflicts of interest.

Figure Legends

Figure 1. A) Characterisation of primary HUVECs from non-GDM and GDM pregnancies using flow cytometry. i) Representative flow cytometry plots to demonstrate the gating strategy applied to remove debris and doublets. Representative flow cytometry plot to demonstrate the gating of CD31+CD144+ HUVECs. **ii)** Percentage of total HUVECs from non-GDM and GDM pregnancies, that co-express CD31 and CD144 (n=3 per group). Data is presented as the mean. **iii)** Histograms of fluorescence minus one (FMO) controls and stained HUVECs from non-GDM and GDM pregnancies expressing CD144 and CD31 (n=3 per group). **B) Expression of EndMT markers in non-GDM and GDM HUVECs.** HUVECs were isolated from non-GDM (n=6) and GDM pregnancies (n=5) and expression of EndMT markers, including endothelial and mesenchymal markers, were measured via RT-qPCR. As a mesenchymal cell positive control primary placental mesenchymal stromal cells (pMSCs) were used. Data is presented as the mean. Statistical analysis was performed using an unpaired t-test (normally distributed), except *TAGLN*, which is presented as the median and statistical analysis was performed using a Mann-Whitney U test (not normally distributed) (* $p<0.05$ in GDM compared to Non-GDM).

Figure 2. A combination of TGF-β2 and IL-1β are optimal for induction of EndMT in HUVECs. HUVECs (Promocell) were cultured in either control medium (EGM-2 only) or treated with EGM-2 containing TGF-β1 (10 ng/mL), TGF-β2 (10 ng/mL), TGF-β1 (10 ng/mL) with IL-1β (10 ng/mL) or TGF-β2 (10 ng/mL) with IL-1β (10 ng/mL) for 6 days (n=3). As a mesenchymal cell positive control primary placental mesenchymal stromal cells (pMSCs) were used. **A)** Morphological images of HUVECs captured using Euromex Oxion Inverso microscope 10x magnification. Scale bars = 100 µm. **B)** Expression of endothelial and mesenchymal genes measured via RT-qPCR. Data is presented as the median. Statistical analysis was performed using a Kruskal-Wallis with a Dunn's post-hoc test between control and treated HUVECs (* $p<0.05$). **C)** Further HUVECs (Promocell) were cultured in either control medium (EGM-2 only) or treated with EGM-2 containing TGF-β2 (10 ng/mL) and of IL-1β (10 ng/mL) for 6 days. As a mesenchymal cell positive control primary placental mesenchymal stromal cells (pMSCs) were used. Gene expression of endothelial and mesenchymal genes measured via RT-qPCR (n=6). Data is presented as the mean. Statistical analysis was performed using an unpaired t-test between control and treated HUVECs (normally distributed), except *TAGLN*, which is presented as the median and statistical analysis was performed using a Mann-Whitney U test (not normally distributed; * $p<0.05$, ** $p<0.01$, *** $p<0.001$, **** $p<0.0001$). **D)** Immunocytochemistry of HUVECs (n=3) and pMSCs stained with CD31, VWF, αSMA and Transgelin, imaged using the Olympus IX83 microscope at 20x magnification. Scale bars = 50 µm. Isotype-specific controls were also used. The same exposure times were used for each antibody across all samples. Further image processing was performed in Qupath (v. 0.5.1), including adjustments for brightness and contrast, where the same settings were for each antibody across all samples.

Figure 3. EndMT can be induced in primary HUVECs from non-GDM and GDM pregnancies. HUVECs isolated from non-GDM (n=6) and GDM pregnancies (n=5) were cultured in either control medium (EGM-2 only) or treated with EGM-2 containing of TGF-β2 (10 ng/mL) and IL-1β (10 ng/mL) for 6 days. As a mesenchymal cell positive control primary placental mesenchymal stromal cells (pMSCs) were used. **A)** Morphological images of HUVECs captured using Euromex Oxion Inverso microscope at 10x magnification. Scale bars = 100 µm. **B)** Expression of endothelial and mesenchymal genes measured via RT-qPCR. Data is presented as the mean. Statistical analysis was performed using two-way ANOVA with a Fisher's post-hoc test (data that were not normally distributed were log-transformed; * $p<0.05$, ** $p<0.01$, *** $p<0.001$, **** $p<0.0001$). **C) and D)** Immunocytochemistry of HUVECs and pMSCs stained with CD31, VWF, VE-Cadherin, αSMA, Transgelin, and Ki67, imaged using the Olympus IX83 microscope at 20x magnification. The same exposure times were used for each antibody across all samples. Further image processing and quantification was performed in Qupath (v. 0.5.1), including adjustments for brightness and contrast, where the same settings were for each antibody across all samples. A pixel classifier threshold was set to detect the cells in each ROI. The fluorescence intensity was then determined using the intensity features tool. The intensity was calculated per pixel, to account for differing numbers and sizes of cells in each ROI/image. For Ki67 analysis, the positive cell detection tool was used to identify total DAPI positive cells, and Ki67 positive cells. Quantification data (**C**) is presented as the mean. Statistical analysis was performed using two-way ANOVA with a Fisher's post-hoc test (data that were not normally distributed were log-transformed; * $p<0.05$, ** $p<0.01$, *** $p<0.001$, **** $p<0.0001$). Representative images are shown (**D**), scale bars = 50 µm.

Figure 4. EndMT induction in GDM HUVECs occurs in a similar manner to non-GDM HUVECs. HUVECs isolated from non-GDM (n=6) and GDM pregnancies (n=5) were cultured in either control medium (EGM-2 only) or treated with EGM-2 containing TGF-β2 (10 ng/mL) and IL-1β (10 ng/mL) for 6 days. As a mesenchymal cell positive control primary placental mesenchymal stromal cells (pMSCs) were used. Expression of EndMT regulators, transcription factors, and signalling molecules were measured via RT-qPCR. Data is presented as the mean. Statistical analysis was performed using two-way ANOVA with a Fisher's post-hoc test (data that were not normally distributed were log-transformed; * $p<0.05$, ** $p<0.01$, *** $p<0.001$, **** $p<0.0001$).

Figure 5. Expression of EndMT markers in non-GDM and GDM placenta. A) Representative images of EndMT markers and mediators, CD31, αSMA, Transgelin, Snail and Slug in term placental tissue from non-GDM and GDM pregnancies. Scale Bars

= 50 µm. **B-C)** Gene expression of endothelial and mesenchymal markers **(B)** and EndMT regulators, transcription factors, and signalling molecules **(C)** in non-GDM (n=16-17) and GDM (n=18-19) human term placenta, measured by RT-qPCR. Data is presented as the median and statistical analysis was performed using a Mann-Whitney U test (not normally distributed), except *SNAI2*, *TGFB3*, *TGFBR1* and *SMAD2* which are presented as the mean and statistical analysis was performed using an unpaired t-test (normally distributed; * $p<0.05$, ** $p<0.01$).

References

Aguilera J, Semmler J, Anzoategui S, Zhang H, Nicolaides KH & Charakida M (2021). Cardiac function in gestational diabetes mellitus: A longitudinal study from fetal life to infancy. *BJOG* **128,** 272–279.

Akarsu S, Bagirzade M, Omeroglu S & Büke B (2017). Placental vascularization and apoptosis in Type-1 and gestational DM. *Journal of Maternal-Fetal and Neonatal Medicine* **30,** 1045–1050.

Al-Biltagi M, El razaky O & El Amrousy D (2021). Cardiac changes in infants of diabetic mothers. *World J Diabetes* **12,** 1233–1247.

Anbara T, Sharifi M & Aboutaleb N (2019). Endothelial to Mesenchymal Transition in the Cardiogenesis and Cardiovascular Diseases. *Curr Cardiol Rev* **16,** 306–314.

Aplin J, Swietlik S, Charnock J, Khalid M, Westwood M & Johnstone E (2015). Vascular regression in the fetoplacental vascular bed, and its possible implications for fetal growth restriction. *Placenta* **36,** 472.

Babawale MO, Lovat S, Mayhew TM, Lammiman MJ, James DK & Leach L (2000). Effects of gestational diabetes on junctional adhesion molecules in human term placental vasculature. *Diabetologia* **43,** 1185–1196.

Balsells M, García-Patterson A, Gich I & Corcoy R (2012). Major congenital malformations in women with gestational diabetes mellitus: A systematic review and meta-analysis. *Diabetes Metab Res Rev* **28,** 252–257.

Bankhead P, Loughrey MB, Fernández JA, Dombrowski Y, McArt DG, Dunne PD, McQuaid S, Gray RT, Murray LJ, Coleman HG, James JA, Salto-Tellez M & Hamilton PW (2017). QuPath: Open source software for digital pathology image analysis. *Sci Rep*; DOI: 10.1038/s41598-017-17204-5.

Bellehumeur C, Blanchet J, Fontaine JY, Bourcier N & Akoum A (2009). Interleukin 1 regulates its own receptors in human endometrial cells via distinct mechanisms. *Human Reproduction* **24,** 2193–2204.

625 Bhattacharjee D, Mondal SK, Garain P, Mandal P, Ray RN & Dey G (2017). Histopathological study with
626 immunohistochemical expression of vascular endothelial growth factor in placentas of
627 hyperglycemic and diabetic women. *J Lab Physicians* **9,** 227–233.

628 Bischoff J (2019). Endothelial-to-Mesenchymal Transition. *Circ Res* **124,** 1163–1165.

629 Böhrnsen F & Schliephake H (2016). Supportive angiogenic and osteogenic differentiation of
630 mesenchymal stromal cells and endothelial cells in monolayer and co-cultures. *Int J Oral Sci* **8,**
631 223–230.

632 Boss AL, Chamley LW, Brooks AES & James JL (2023). Human placental vascular and perivascular cell
633 heterogeneity differs between first trimester and term, and in pregnancies affected by foetal
634 growth restriction. *Mol Hum Reprod*; DOI: 10.1093/molehr/gaad041.

635 Briana DD, Liosi S, Gourgiotis D, Boutsikou M, Marmarinos A, Baka S, Hassiakos D & Malamitsi-Puchner
636 A (2012). Fetal concentrations of the growth factors TGF-α and TGF-β1 in relation to normal and
637 restricted fetal growth at term. *Cytokine* **60,** 157–161.

638 Bronson R, Lyu J & Xiong J (2023). Transcriptome analysis reveals molecular signature and cell-type
639 difference of Homo sapiens endothelial-to-mesenchymal transition. *G3: Genes, Genomes,*
640 *Genetics*; DOI: 10.1093/g3journal/jkad243.

641 Byford A, Baird-Rayner C & Forbes K (2021). Don't sugar coat it: the effects of gestational diabetes on
642 the placental vasculature. *Biochem (Lond)* **43,** 34–39.

643 Calderon IMP, Damasceno DC, Amorin RL, Costa RAA, Brasil MAM & Rudge MVC (2007).
644 Morphometric study of placental villi and vessels in women with mild hyperglycemia or
645 gestational or overt diabetes. *Diabetes Res Clin Pract* **78,** 65–71.

646 Castrechini NM, Murthi P, Gude NM, Erwich JJHM, Gronthos S, Zannettino A, Brennecke SP & Kalionis
647 B (2010). Mesenchymal stem cells in human placental chorionic villi reside in a vascular Niche.
648 *Placenta* **31,** 203–212.

649 Charnock-Jones DS & Burton GJ (2000). Placental vascular morphogenesis. *Best Pract Res Clin Obstet*
650 *Gynaecol* **14,** 953–968.

651 Charnock-Jones DS, Kaufmann P & Mayhew TM (2004). Aspects of human fetoplacental
652 vasculogenesis and angiogenesis. I. Molecular regulation. *Placenta* **25,** 103–113.

653 Chen A, Tan B, Du R, Chong YS, Zhang C, Koh AS & Li LJ (2024). Gestational diabetes mellitus and
654 development of intergenerational overall and subtypes of cardiovascular diseases: a systematic
655 review and meta-analysis. *Cardiovasc Diabetol* **23,** 1–15.

656 Chen DB & Zheng J (2014). Regulation of Placental Angiogenesis. *Microcirculation* **21,** 15–25.

657 Chen L, He J, Zhang Y, Li Y, Zhang T, Wang R, Bai L, Zhao S, Liu E & Wang W (2023). Regulation of
658 endothelial-to-mesenchymal transition by histone deacetylase 3 posttranslational modifications
659 in neointimal hyperplasia. *Ann Transl Med* **11,** 207–207.

660 Cvitic S, Novakovic B, Gordon L, Ulz CM, Mühlberger M, Diaz-Perez FI, Joo JE, Svendova V, Schimek
661 MG, Trajanoski S, Saffery R, Desoye G & Hiden U (2018). Human fetoplacental arterial and venous
662 endothelial cells are differentially programmed by gestational diabetes mellitus, resulting in cell-
663 specific barrier function changes. *Diabetologia* **61,** 2398–2411.

664 Daskalakis G, Marinopoulos S, Krielesi V, Papapanagiotou A, Papantoniou N, Mesogitis S & Antsaklis A
665 (2008). Placental pathology in women with gestational diabetes. *Acta Obstet Gynecol Scand* **87,**
666 403–407.

667 Demir R, Seval Y & Huppertz B (2007). Vasculogenesis and angiogenesis in the early human placenta.
668 *Acta Histochem* **109,** 257–265.

669 Depla AL, De Wit L, Steenhuis TJ, Slieker MG, Voormolen DN, Scheffer PG, De Heus R, Van Rijn BB &
670 Bekker MN (2021). Effect of maternal diabetes on fetal heart function on echocardiography:
671 systematic review and meta-analysis. *Ultrasound Obstet Gynecol* **57,** 539–550.

672 Diniz MS, Hiden U, Falcão-Pires I, Oliveira PJ, Sobrevia L & Pereira SP (2023). Fetoplacental endothelial
673 dysfunction in gestational diabetes mellitus and maternal obesity: A potential threat for
674 programming cardiovascular disease. *Biochim Biophys Acta Mol Basis Dis*; DOI:
675 10.1016/j.bbadis.2023.166834.

676 Drever HJ, Davidson SJ, Callaway LK, Sekar R & De Jersey SJ (2023). Factors associated with higher risk
677 of small-for-gestational-age infants in women treated for gestational diabetes. *Australian and*
678 *New Zealand Journal of Obstetrics and Gynaecology* **63,** 714–720.

679 Dusza HM, van Boxel J, van Duursen MBM, Forsberg MM, Legler J & Vähäkangas KH (2023).
680 Experimental human placental models for studying uptake, transport and toxicity of micro- and
681 nanoplastics. *Science of The Total Environment* **860,** 160403.

682 Ehlers E, Talton OO, Schust DJ & Schulz LC (2021). Placental structural abnormalities in gestational
683 diabetes and when they develop: A scoping review. *Placenta* **116,** 58–66.

684 Evrard SM et al. (2016). Endothelial to mesenchymal transition is common in atherosclerotic lesions
685 and is associated with plaque instability. *Nat Commun*; DOI: 10.1038/ncomms11853.

686 Fahey E & Doyle SL (2019). IL-1 family cytokine regulation of vascular permeability and angiogenesis.
687 *Front Immunol*; DOI: 10.3389/fimmu.2019.01426.

688 Ferreira FU, Souza LEB, Thomé CH, Pinto MT, Origassa C, Salustiano S, Faça VM, Câmara NO, Kashima
689 S & Covas DT (2019). Endothelial cells tissue-specific origins affects their responsiveness to TGF-
690 β2 during endothelial-to-mesenchymal transition. *Int J Mol Sci*; DOI: 10.3390/ijms20030458.

691 Forbes K, Westwood M, Baker PN & Aplin JD (2008). Insulin-like growth factor I and II regulate the life
692 cycle of trophoblast in the developing human placenta. *Am J Physiol Cell Physiol* **294,** 1313–1322.

693 Fu TL, Li GR, Li DH, He RY, Liu BH, Xiong R, Xu CZ, Lu ZL, Song CK, Qiu HL, Wang WJ, Zou SS, Yi K, Li N &
694 Geng Q (2024). Mangiferin alleviates diabetic pulmonary fibrosis in mice via inhibiting

endothelial-mesenchymal transition through AMPK/FoxO3/SIRT3 axis. *Acta Pharmacol Sin* **45,** 1002–1018.

Gordon B, González-Fernández V & Dos-Subirà L (2022). Myocardial fibrosis in congenital heart disease. *Front Pediatr*; DOI: 10.3389/fped.2022.965204.

Goumans M, Valdimarsdottir G, Itoh S, Rosendahl A, Sideras P & ten Dijke P (2002). Balancing the activation state of the endothelium via two distinct TGF-β type I receptors. *EMBO J* **21,** 1743-1753–1753.

Goumans MJ, Liu Z & Ten Dijke P (2009). TGF-β signaling in vascular biology and dysfunction. *Cell Res* **19,** 116–127.

Grissa O, Yessoufou A, Mrisak I, Hichami A, Amoussou-Guenou D, Grissa A, Djrolo F, Moutairou K, Miled A, Khairi H, Zaouali M, Bougmiza I, Zbidi A, Tabka Z & Khan NA (2010). Growth factor concentrations and their placental mRNA expression are modulated in gestational diabetes mellitus: Possible interactions with macrosomia. *BMC Pregnancy Childbirth*; DOI: 10.1186/1471-2393-10-7.

Helle EIT, Biegley P, Knowles JW, Leader JB, Pendergrass S, Yang W, Reaven GR, Shaw GM, Ritchie M & Priest JR (2018). First Trimester Plasma Glucose Values in Women without Diabetes are Associated with Risk for Congenital Heart Disease in Offspring. *Journal of Pediatrics* **195,** 275–278.

Holme AM, Roland MCP, Lorentzen B, Michelsen TM & Henriksen T (2015). Placental glucose transfer: A human in vivo study. *PLoS One*; DOI: 10.1371/journal.pone.0117084.

Hulshoff MS, Schellinger IN, Xu X, Fledderus J, Rath SK, Wong FC, Maamari S, Haunschild J, Krenning G, Raaz U & Zeisberg EM (2023). miR-132-3p and KLF7 as novel regulators of aortic stiffening-associated EndMT in type 2 diabetes mellitus. *Diabetol Metab Syndr*; DOI: 10.1186/s13098-022-00966-y.

James JL, Boss AL, Sun C, Allerkamp HH & Clark AR (2022). From stem cells to spiral arteries: A journey through early placental development. *Placenta* **125,** 68–77.

Jirkovská M, Kučera T, Kaláb J, Jadrníček M, Niedobová V, Janáček J, Kubínová L, Moravcová M, Žižka Z & Krejčí V (2012). The branching pattern of villous capillaries and structural changes of placental terminal villi in type 1 diabetes mellitus. *Placenta* **33,** 343–351.

Junaid TO, Brownbill P, Chalmers N, Johnstone ED & Aplin JD (2014). Fetoplacental vascular alterations associated with fetal growth restriction. *Placenta* **35,** 808–815.

Kennedy MG (2022). *Circulating miRNAs as key regulators of placental vascular dysfunction and altered fetal growth in pregnancies complicated by diabetes* (thesis). University of Leeds.

Kovacic JC, Dimmeler S, Harvey RP, Finkel T, Aikawa E, Krenning G & Baker AH (2019). Endothelial to Mesenchymal Transition in Cardiovascular Disease: JACC State-of-the-Art Review. *J Am Coll Cardiol* **73,** 190–209.

Kramer CK, Campbell S & Retnakaran R (2019). Gestational diabetes and the risk of cardiovascular disease in women: a systematic review and meta-analysis. *Diabetologia* **62,** 905–914.

Lang I, Hartmann M, Blaschitz A, Dohr G, Skofitsch G & Desoye G (1993). Immunohistochemical evidence for the heterogeneity of maternal and fetal vascular endothelial cells in human full-term placenta. *Cell Tissue Res* **274,** 211–218.

Lang I, Schweizer A, Hiden U, Ghaffari-Tabrizi N, Hagendorfer G, Bilban M, Pabst MA, Korgun ET, Dohr G & Desoye G (2008). Human fetal placental endothelial cells have a mature arterial and a juvenile venous phenotype with adipogenic and osteogenic differentiation potential. *Differentiation* **76,** 1031–1043.

Law GR, Alnaji A, Alrefaii L, Endersby D, Cartland SJ, Gilbey SG, Jennings PE, Murphy HR & Scott EM (2019). Suboptimal nocturnal glucose control is associated with large for gestational age in treated gestational diabetes mellitus. *Diabetes Care* **42,** 810–815.

743 Leach L, Babawale MO, Anderson M & Lammiman M (2002). Vasculogenesis, angiogenesis and the
744 molecular organisation of endothelial junctions in the early human placenta. *J Vasc Res* **39,** 246–
745 259.

746 Leach L, Gray C, Staton S, Babawale MO, Gruchy A, Foster C, Mayhew TM & James DK (2004). Vascular
747 endothelial cadherin and β-catenin in human fetoplacental vessels of pregnancies complicated
748 by Type 1 diabetes: Associations with angiogenesis and perturbed barrier function. *Diabetologia*
749 **47,** 695–709.

750 Li Y, Zhao Y, Song L, Xiong L, Li W, Wu W & Miao L (2023). High glucose levels contribute to vascular
751 fibrosis via the activation of the endothelial-to-mesenchymal transition in periodontitis. *J*
752 *Periodontal Res* **58,** 225–236.

753 Liu Y, Yue L & Chang L (2024). Maternal Gestational Diabetes Mellitus and Congenital Heart Disease in
754 Offspring: A Meta-Analysis. *Hormone and Metabolic Research* **56,** 574–584.

755 Ma J, van der Zon G, Gonçalves MAFV, van Dinther M, Thorikay M, Sanchez-Duffhues G & ten Dijke P
756 (2021). TGF-β-Induced Endothelial to Mesenchymal Transition Is Determined by a Balance
757 Between SNAIL and ID Factors. *Front Cell Dev Biol*; DOI: 10.3389/fcell.2021.616610.

758 Mahadevan A, Tipler A & Jones H (2023). Shared developmental pathways of the placenta and fetal
759 heart. *Placenta* **141,** 35–42.

760 Maleszewska M, Moonen JRAJ, Huijkman N, van de Sluis B, Krenning G & Harmsen MC (2013). IL-1β
761 and TGFβ2 synergistically induce endothelial to mesenchymal transition in an NFκB-dependent
762 manner. *Immunobiology* **218,** 443–454.

763 Markwald RR, Fitzharris TP & Manasek FJ (1977). Structural development of endocardial cushions.
764 *American Journal of Anatomy* **148,** 85–119.

765 Markwald RR, Fitzharris TP & Smithy WNA (1975). *Structural Analysis of Endocardial*
766 *Cytodifferentiation I*.

767 Di Matteo S et al. (2021). Metformin exerts anti-cancerogenic effects and reverses epithelial-to-
768 mesenchymal transition trait in primary human intrahepatic cholangiocarcinoma cells. *Sci Rep*;
769 DOI: 10.1038/s41598-021-81172-0.

770 Meng Z, Shen W, Yu L, Tong F, He H, Hu Y, Wu W & Liu J (2023). Bach1 modulates AKT3 transcription
771 to participate in hyperglycaemia-mediated EndMT in vascular endothelial cells. *Clin Exp*
772 *Pharmacol Physiol* **50,** 443–452.

773 Metzger BE et al. (2008). Hyperglycemia and adverse pregnancy outcomes. *New England Journal of*
774 *Medicine* **358,** 1991–2002.

775 Monteiro JP et al. (2021). MIR503HG Loss Promotes Endothelial-to-Mesenchymal Transition in
776 Vascular Disease. *Circ Res* **128,** 1173–1190.

777 Morrison MJ, Natale B V., Allen S, Peterson N & Natale DRC (2024). Characterizing placental pericytes:
778 Hypoxia and proangiogenic signalling. *Placenta* **155,** 1–10.

779 Mrizak I, Grissa O, Henault B, Fekih M, Bouslema A, Boumaiza I, Zaouali M, Tabka Z & Khan NA (2014).
780 Placental infiltration of inflammatory markers in gestational diabetic women. *Gen Physiol*
781 *Biophys* **33,** 169–176.

782 NICE (2015). New thresholds for diagnosis of diabetes in pregnancy. Available at:
783 https://www.nice.org.uk/news/article/new-thresholds-for-diagnosis-of-diabetes-in-pregnancy
784 [Accessed May 13, 2020].

785 Pelekanos RA, Sardesai VS, Futrega K, Lott WB, Kuhn M & Doran MR (2016). Isolation and expansion
786 of mesenchymal stem/stromal cells derived from human placenta tissue. *Journal of Visualized*
787 *Experiments* **2016,** 1–3.

788 Pérez L, Muñoz-Durango N, Riedel CA, Echeverría C, Kalergis AM, Cabello-Verrugio C & Simon F (2017).
789 Endothelial-to-mesenchymal transition: Cytokine-mediated pathways that determine
790 endothelial fibrosis under inflammatory conditions. *Cytokine Growth Factor Rev* **33,** 41–54.

791 Piera-Velazquez S & Jimenez SA (2019). Endothelial to Mesenchymal Transition: Role in Physiology
792 and in the Pathogenesis of Human Diseases. *Physiol Rev* **99,** 1281–1324.

793 Pinto MT, Covas DT, Kashima S & Rodrigues CO (2016). Endothelial Mesenchymal Transition:
794 Comparative Analysis of Different Induction Methods. *Biol Proced Online* **18,** 1–8.

795 Seval Y, Korgun ET & Demir R (2007). Hofbauer Cells in Early Human Placenta: Possible Implications in
796 Vasculogenesis and Angiogenesis. *Placenta* **28,** 841–845.

797 Shen C, Lie P, Miao T, Yu M, Lu Q, Feng T, Li J, Zu T, Liu X & Li H (2015). Conditioned medium from
798 umbilical cord mesenchymal stem cells induces migration and angiogenesis. *Mol Med Rep* **12,**
799 20–30.

800 Singh A, Bhatt KS, Nguyen HC, Frisbee JC & Singh KK (2024). Endothelial-to-Mesenchymal Transition
801 in Cardiovascular Pathophysiology. *Int J Mol Sci*; DOI: 10.3390/ijms25116180.

802 Sobrevia L, Abarzúa F, Nien JK, Salomón C, Westermeier F, Puebla C, Cifuentes F, Guzmán-Gutiérrez E,
803 Leiva A & Casanello P (2011). Review: Differential placental macrovascular and microvascular
804 endothelial dysfunction in gestational diabetes. *Placenta* **32 Suppl 2,** S159-64.

805 Stoz F, Schuhmann RA & Schultz R (1988). Morphohistometric investigations of placentas of diabetic
806 patients in correlation to the metabolic adjustment of the disease. *J Perinat Med* **16,** 211–216.

807 Tagoma A, Haller-Kikkatalo K, Oras A, Roos K, Kirss A & Uibo R (2022). Plasma cytokines during
808 pregnancy provide insight into the risk of diabetes in the gestational diabetes risk group. *J*
809 *Diabetes Investig* **13,** 1596–1606.

810 Terzuoli E, Nannelli G, Giachetti A, Morbidelli L, Ziche M & Donnini S (2020). Targeting endothelial-to-
811 mesenchymal transition: the protective role of hydroxytyrosol sulfate metabolite. *Eur J Nutr* **59,**
812 517–527.

Tian J, Zhang M, Suo M, Liu D, Wang X, Liu M, Pan J, Jin T & An F (2021). Dapagliflozin alleviates cardiac fibrosis through suppressing EndMT and fibroblast activation via AMPKα/TGF-β/Smad signalling in type 2 diabetic rats. *J Cell Mol Med* **25,** 7642–7659.

Troncoso F, Acurio J, Herlitz K, Aguayo C, Bertoglia P, Guzman-Gutierrez E, Loyola M, Gonzalez M, Rezgaoui M, Desoye G & Escudero C (2017). Gestational diabetes mellitus is associated with increased pro-migratory activation of vascular endothelial growth factor receptor 2 and reduced expression of vascular endothelial growth factor receptor 1. *PLoS One*; DOI: 10.1371/journal.pone.0182509.

Tsai TH, Lee CH, Cheng CI, Fang YN, Chung SY, Chen SM, Lin CJ, Wu CJ, Hang CL & Chen WY (2019). Liraglutide inhibits endothelial-to-mesenchymal transition and attenuates neointima formation after endovascular injury in streptozotocin-induced diabetic mice. *Cells*; DOI: 10.3390/cells8060589.

Vega-Tapia F, Peñaloza E & Krause BJ (2021). Specific arterio-venous transcriptomic and ncRNA-RNA interactions in human umbilical endothelial cells: A meta-analysis. *iScience*; DOI: 10.1016/j.isci.2021.102675.

Venkataraman H, Ram U, Craik S, Arungunasekaran A, Seshadri S & Saravanan P (2016). Increased fetal adiposity prior to diagnosis of gestational diabetes in South Asians: more evidence for the 'thin–fat' baby. *Diabetologia* **60,** 399.

Villota SD, Toledo-Rodriguez M & Leach L (2021). Compromised barrier integrity of human feto-placental vessels from gestational diabetic pregnancies is related to downregulation of occludin expression. *Diabetologia* **64,** 195–210.

Vitoratos N, Professor A, Vitoratos N, Valsamakis G, Mastorakos G, Boutsiadis A, Salakos N, Kouskouni E & Creatsas G (2008). *Pre-and early post-partum adiponectin and Interleukin-1beta levels in women with and without gestational diabetes*.

Wang C, Li Y, Yang M, Zou Y, Liu H, Liang Z, Yin Y, Niu G, Yan Z & Zhang B (2018). Efficient Differentiation of Bone Marrow Mesenchymal Stem Cells into Endothelial Cells in Vitro. *European Journal of Vascular and Endovascular Surgery* **55,** 257–265.

Wang E, Wang H & Chakrabarti S (2023*a*). Endothelial-to-mesenchymal transition: An underappreciated mediator of diabetic complications. *Front Endocrinol (Lausanne)*; DOI: 10.3389/fendo.2023.1050540.

Wang H, Li N, Chivese T, Werfalli M, Sun H, Yuen L, Hoegfeldt CA, Elise Powe C, Immanuel J, Karuranga S, Divakar H, Levitt NaA, Li C, Simmons D & Yang X (2022). IDF Diabetes Atlas: Estimation of Global and Regional Gestational Diabetes Mellitus Prevalence for 2021 by International Association of Diabetes in Pregnancy Study Group's Criteria. *Diabetes Res Clin Pract* **183,** 109050.

Wang JJ, Wang X, Li Q, Huang H, Zheng QL, Yao Q & Zhang J (2023*b*). Feto-placental endothelial dysfunction in Gestational Diabetes Mellitus under dietary or insulin therapy. *BMC Endocr Disord*; DOI: 10.1186/S12902-023-01305-6.

Wang Y & Zhao S (2010). *Vascular Biology of the Placenta*.

Xu X, Tan X, Tampe B, Sanchez E, Zeisberg M & Zeisberg EM (2015). Snail Is a direct target of hypoxia-inducible factor 1α (HIF1α) in hypoxia-induced endothelial to mesenchymal transition of human coronary endothelial cells. *Journal of Biological Chemistry* **290,** 16553–16664.

Yener S, Demir T, Akinci B, Bayraktar F, Kebapcilar L, Ozcan MA, Biberoglu S & Yesil S (2007). Transforming growth factor-beta 1 levels in women with prior history of gestational diabetes mellitus. *Diabetes Res Clin Pract* **76,** 193–198.

Yoshimatsu Y, Wakabayashi I, Kimuro S, Takahashi N, Takahashi K, Kobayashi M, Maishi N, Podyma-Inoue KA, Hida K, Miyazono K & Watabe T (2020). TNF-α enhances TGF-β-induced endothelial-to-mesenchymal transition via TGF-β signal augmentation. *Cancer Sci* **111,** 2385–2399.

Yu H, Mrowietz U & Seifert O (2009). Downregulation of SMAD2, 4 and 6 mRNA and TGFβ receptor I mRNA in lesional and non-lesional psoriatic skin. *Acta Derm Venereol* **89,** 351–356.

Zgutka K, Tkacz M, Tomasiak P, Piotrowska K, Ustianowski P, Pawlik A & Tarnowski M (2024). Gestational Diabetes Mellitus-Induced Inflammation in the Placenta via IL-1β and Toll-like Receptor Pathways. *Int J Mol Sci* **25,** 11409.

Zhang Y, Alexander PB & Wang XF (2017). TGF-β family signaling in the control of cell proliferation and survival. *Cold Spring Harb Perspect Biol*; DOI: 10.1101/cshperspect.a022145.

Zhou J, Ni X, Huang X, Yao J, He Q, Wang K & Duan T (2016). Potential Role of Hyperglycemia in Fetoplacental Endothelial Dysfunction in Gestational Diabetes Mellitus. *Cell Physiol Biochem* **39,** 1317–1328.

Zhou W, Gross KM & Kuperwasser C (2019). Molecular regulation of Snai2 in development and disease. *J Cell Sci*; DOI: 10.1242/jcs.235127.

Zhu X et al. (2023). Acetate controls endothelial-to-mesenchymal transition. *Cell Metab* **35,** 1163-1178.e10.

Figure 1

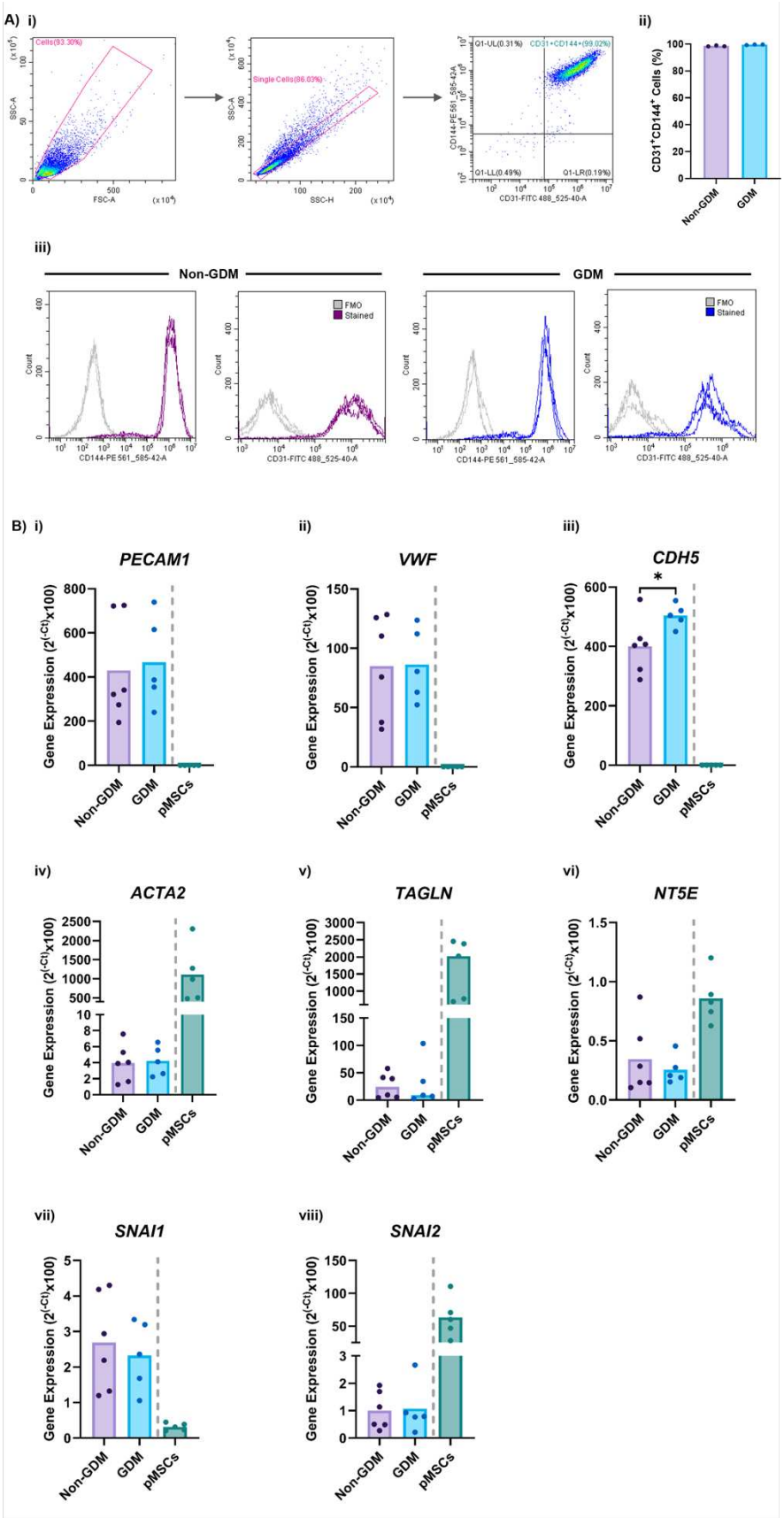
A) i)
Cells(93.30%)
Single Cells(86.03%)
Q1-UL(0.31%)
CD31+CD144+(99.02%)
Q1-LL(0.49%)
Q1-LR(0.19%)
ii)
CD31+CD144+ Cells (%)
Non-GDM
GDM
iii)
Non-GDM
GDM
FMO
Stained
B) i)
PECAM1
ii)
VWF
iii)
CDH5
iv)
ACTA2
v)
TAGLN
vi)
NT5E
vii)
SNAI1
viii)
SNAI2
Gene Expression (2(-Ct))x100
Non-GDM
GDM
pMSCs

883

Figure 2

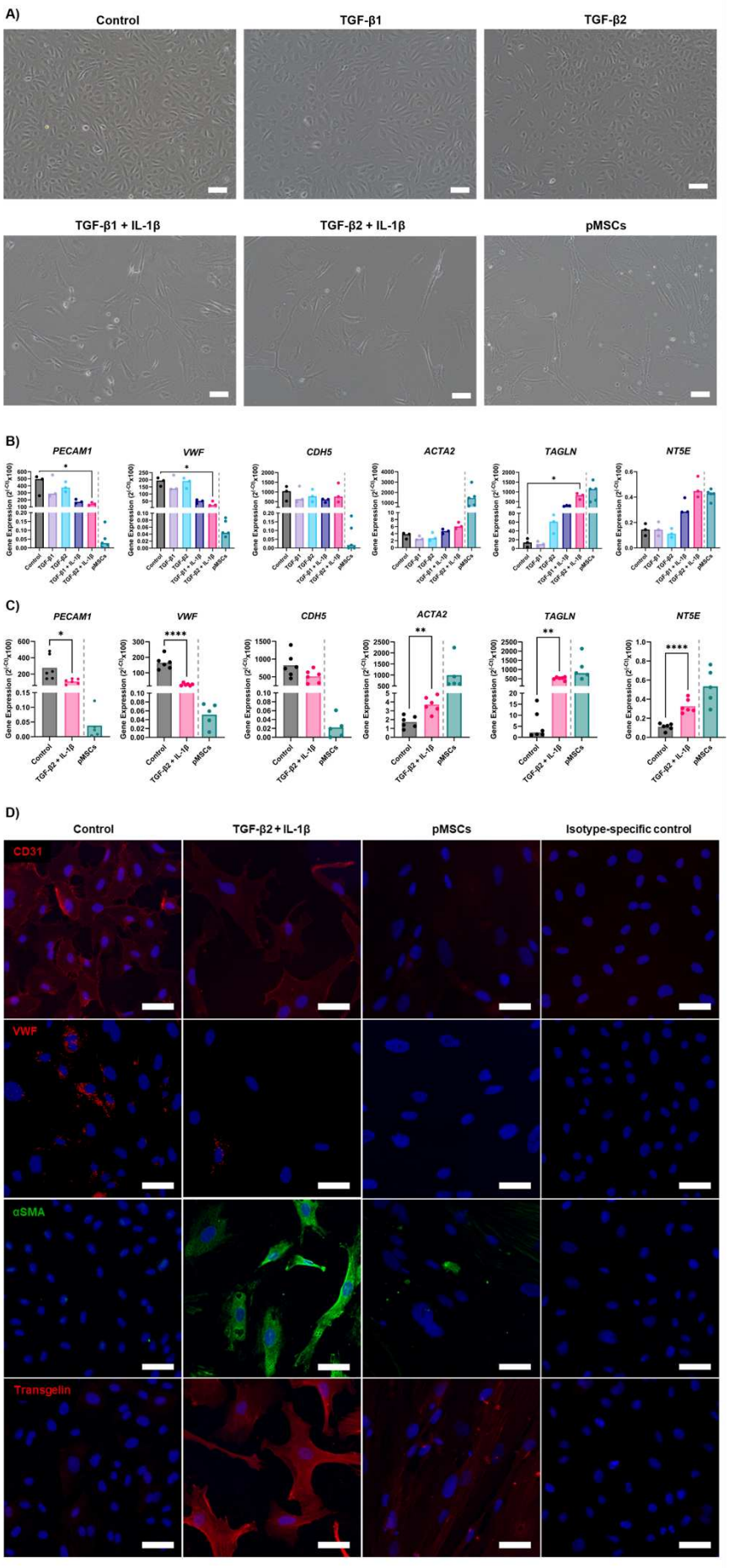
A)
Control
TGF-β1
TGF-β2
TGF-β1 + IL-1β
TGF-β2 + IL-1β
pMSCs
B)
PECAM1
VWF
CDH5
ACTA2
TAGLN
NT5E
C)
PECAM1
VWF
CDH5
ACTA2
TAGLN
NT5E
Control
TGF-β2 + IL-1β
pMSCs
D)
Control
TGF-β2 + IL-1β
pMSCs
Isotype-specific control
CD31
VWF
αSMA
Transgelin

884

Figure 3

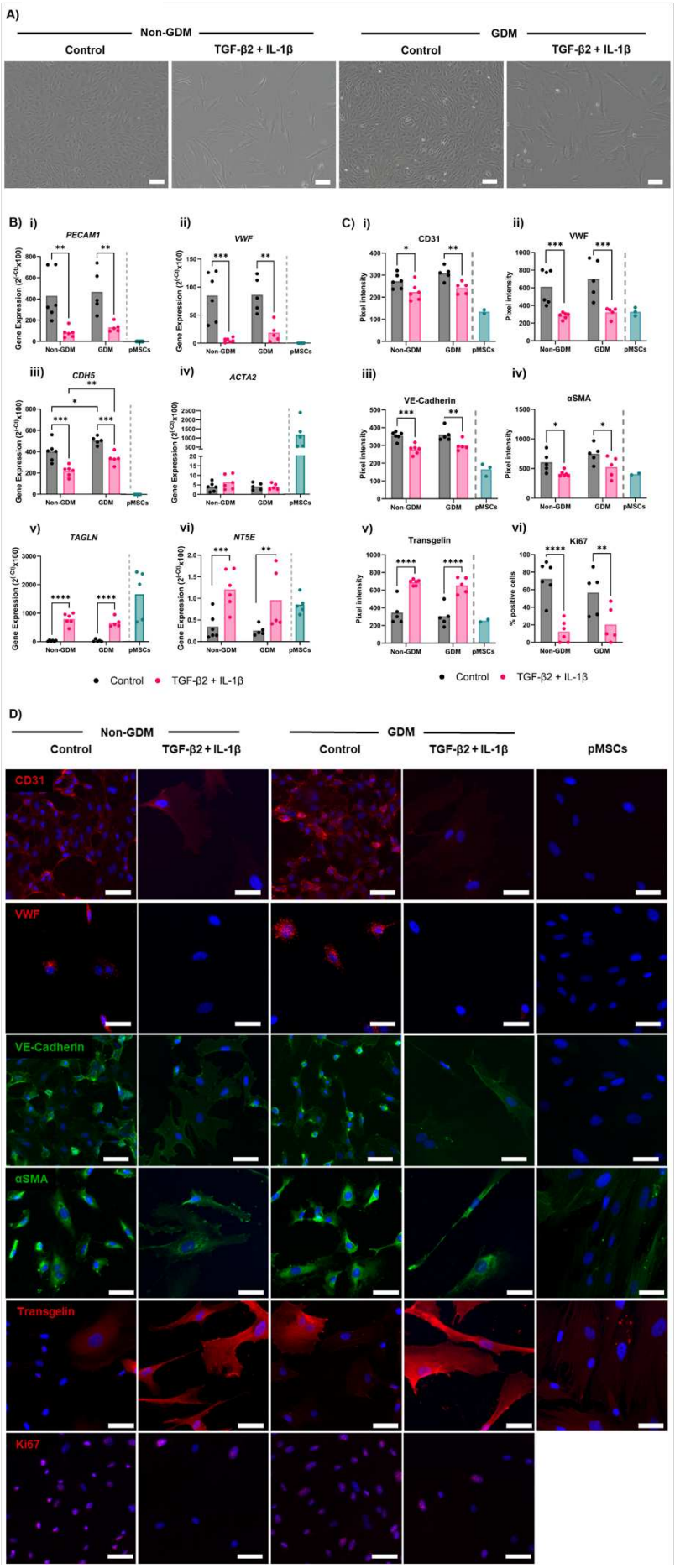
A)
Non-GDM
GDM
Control
TGF-β2 + IL-1β
Control
TGF-β2 + IL-1β
B) i)
PECAM1
ii)
VWF
iii)
CDH5
iv)
ACTA2
v)
TAGLN
vi)
NT5E
Gene Expression (2^-Cq)x100)
Non-GDM
GDM
pMSCs
C) i)
CD31
ii)
VWF
iii)
VE-Cadherin
iv)
αSMA
v)
Transgelin
vi)
Ki67
Pixel intensity
% positive cells
Control
TGF-β2 + IL-1β
D)
Non-GDM
GDM
Control
TGF-β2 + IL-1β
Control
TGF-β2 + IL-1β
pMSCs
CD31
VWF
VE-Cadherin
αSMA
Transgelin
Ki67

Figure 4

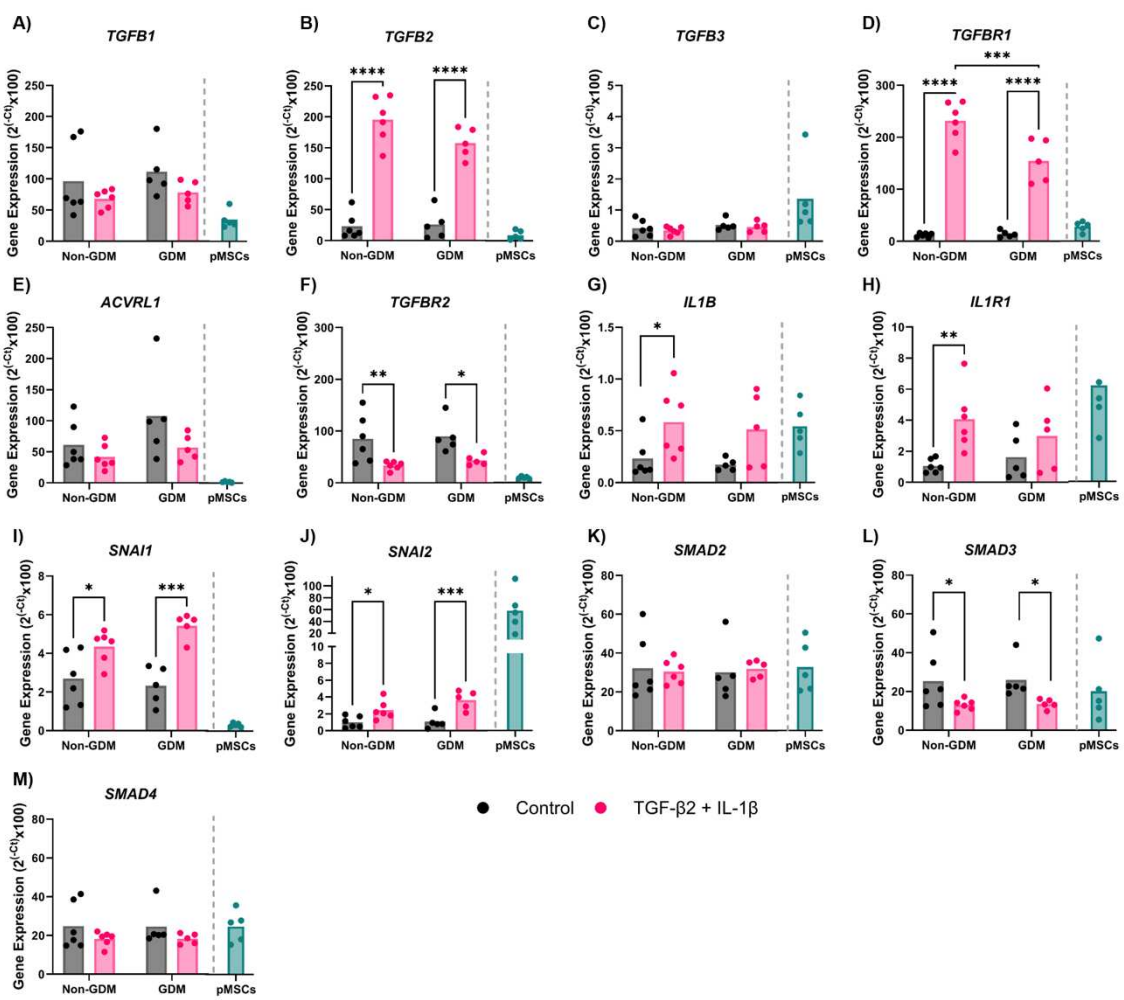
A)
TGFB1
B)
TGFB2
C)
TGFB3
D)
TGFBR1
E)
ACVRL1
F)
TGFBR2
G)
IL1B
H)
IL1R1
I)
SNAI1
J)
SNAI2
K)
SMAD2
L)
SMAD3
M)
SMAD4
Gene Expression (2^(-Ct))x100)
Non-GDM
GDM
pMSCs
Control
TGF-β2 + IL-1β

886

Figure 5

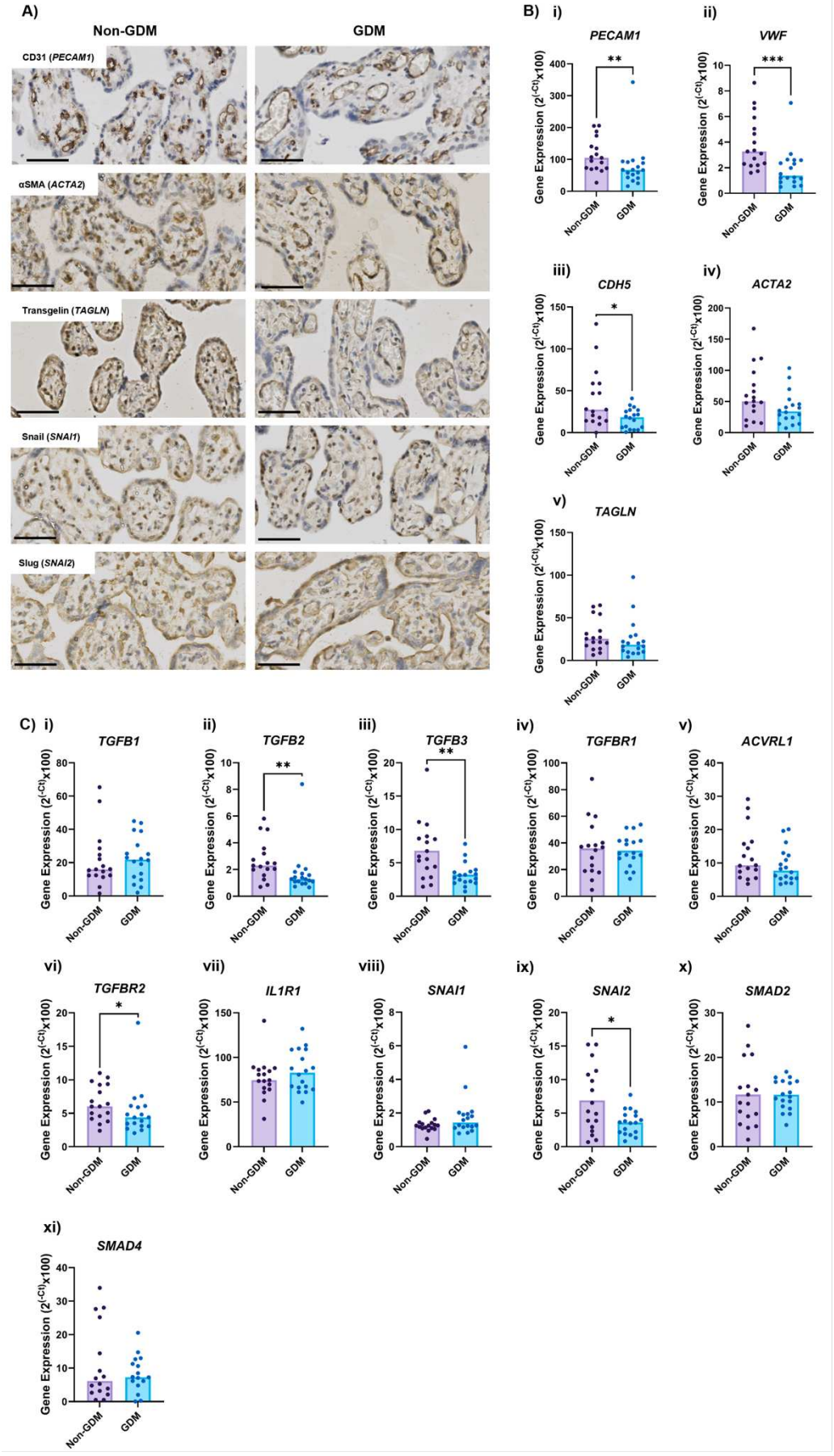
A)
Non-GDM
GDM
CD31 (PECAM1)
αSMA (ACTA2)
Transgelin (TAGLN)
Snail (SNAI1)
Slug (SNAI2)
B) i)
PECAM1
ii)
VWF
iii)
CDH5
iv)
ACTA2
v)
TAGLN
Gene Expression (2^(-Ct))x100)
Non-GDM
GDM
C) i)
TGFB1
ii)
TGFB2
iii)
TGFB3
iv)
TGFBR1
v)
ACVRL1
vi)
TGFBR2
vii)
IL1R1
viii)
SNAI1
ix)
SNAI2
x)
SMAD2
xi)
SMAD4

887